https://doi.org/10.5194/amt-2022-323
Preprint. Discussion started: 14 December 2022

Atmospheric Measurement Techniques Discussions

Insights into 3D cloud radiative transfer for OCO-2

Steven. T. Massie[1], Heather Cronk[2], Aronne Merrelli[3], Sebastian Schmidt[1], and Steffen Mauceri[4]

[1]Laboratory for Atmospheric and Space Physics, University of Colorado, Boulder, Colorado, 80303, USA
[2]Cooperative Institute for Research in the Atmosphere, Colorado State University, Fort Collins, Colorado, 80523, USA
[3]Department of Climate and Space Sciences and Engineering, University of Michigan, Ann Arbor, Michigan, 48109-2143, USA
[4]Jet Propulsion Laboratory, California Institute of Technology, Pasadena, California, 91109, USA

Correspondence to: Steven T Massie (Steven.Massie@lasp.colorado.edu)

Abstract. Clouds impose radiance perturbations upon Orbiting Carbon Observatory (OCO-2) measured spectra. The Spherical Harmonic Discrete Ordinate radiative transfer Method (SHDOM) code is applied in both idealized bar cloud and scene specific calculations of 1D and 3D radiances in order to understand 3D cloud effects for a wide range of gas vertical optical depths, solar and sensor viewing geometries, for ocean and land scenes. We find that OCO-2 measurements are susceptible to 3D cloud effects since 3D radiance enhancements are several times larger than radiance perturbations due to a 1 ppm increase in XCO2, and the 3D radiance perturbations are spectrally distinct (different than the radiance perturbations due to changes in surface pressure, XCO2, aerosol, and surface reflectance). SHDOM calculations for 36 scenes over the Amazon and the Pacific are co-analyzed with Moderate Resolution Imaging Spectroradiometer (MODIS) radiance-based cloud distance data, and OCO-2 Lite file rawXCO2 for both Quality Flag=0, (QF0, best quality) and Quality Flag=1 (QF1, poor quality) data. SHDOM calculations of the ocean and land scenes indicate that the 1 D / 3 D radiance intensity ratios and XCO2 decrease concurrently as nearest cloud distance decreases towards zero, especially for the ocean glint QF1 data, which provide the clearest evidence of 3D cloud effects in OCO-2 retrievals. Average differences in rawXCO2 at cloud distances near 20 and 0 km are an appropriate measure of 3D cloud effect biases (that are introduced by the retrieval), and are calculated for 10° latitude bands for 2015-2018. The ocean glint QF0 (QF1) latitude average 3D rawXCO2 biases are near 0.4 (1.5) ppm.

1 Introduction

The Orbiting Carbon Observatory (OCO-2) measures the column-averaged atmospheric CO_2 dry air mole fraction, referred to as XCO2, on a global basis (Eldering et al., 2017). The measurement goal is to obtain measurements of XCO2 to the 0.25 % level, corresponding to a XCO2 accuracy of 1 ppm, since ambient XCO2 is near 400 ppm.

The OCO-2 instrument is comprised of three spectrometers centered in the O2 A-band (0.76 μm), weak CO_2 band (WCO2, 1.6 μm), and strong CO_2 band (SCO2, 2.06 μm). Spectral resolution $\lambda/\Delta\lambda > 17{,}000$ (Crisp et al., 2017) ensures that individual spectral lines are observed. Each band contains 1016 data points, covering a wide range of optical depth. The OCO-2 experiment has several observing modes: ocean glint, land glint, land nadir, and target mode. In target mode the spectrometers are commanded to observe a specific small geographical region. In ocean glint

https://doi.org/10.5194/amt-2022-323
Preprint. Discussion started: 14 December 2022

Atmospheric Measurement Techniques Discussions

observations the bright ocean glint spot is utilized to increase the observed radiance level. Land glint observations utilize glint observing geometry, and are not restricted to water surfaces. The land nadir observations have a sensor view angle near 0.3°. We focus on ocean glint, land glint, and land nadir scenes in this paper.

The retrieval of XCO2 is based upon the measurement of surface pressure in the O2 A-band, and XCO2 in the WCO2 and SCO2 bands. The retrieval applies the optimal estimation retrieval methodology of Rodgers (2000). The operational retrieval (OCO-2 L2 ATBD, 2020; O'Dell et al., 2018) solves for a state vector with many elements including XCO2, surface pressure, reflectance, and aerosol. Spectroscopic line cross sections for O_2, CO_2, and H_2O are specified by the ABSCO data files (Payne et al. 2020). Payne et al. (2020) discusses the advances in laboratory measurements which deal with difficult spectroscopic issues such as line-mixing and speed dependent line shapes.

XCO2 generated by the operational retrieval is referred to as *raw* XCO2. A post-retrieval processing step then bias corrects the raw XCO2, yielding *bias corrected* XCO2 (bc). Bias correction (O'Dell et al, 2018) is achieved by comparing raw XCO2 to truth proxies: ground based XCO2, measured by the Total Carbon Column Observation Network (TCCON, Wunsch et al. 2017), ensemble model XCO2, and small area analysis (in which differences of XCO2 values and the area average are calculated). The differences between the raw XCO2 and the truth proxies are related in a linear manner to several bias correction parameters (dP over the ocean, dPfrac over land, CO2graddel, and DWS). dP is the difference (in hPa) between the retrieved (Pretrieved) and a priori (Papriori) surface pressure evaluated at the strong SCO2 band geographic location, while dPfrac (in ppm) is

$$\text{dPfrac} = \text{raw XCO2}\ (1.00 - \text{Papriori} / \text{Pretrieved}) \quad (1)$$

CO2graddel is a measure of the difference in the retrieved and prior CO_2 vertical gradient. DWS is the sum of the vertical optical depths of the dust, water, and sea salt aerosol components. The bias correction process takes the raw XCO2 and increases these values by approximately 2 ppm. The need to bias correct is due to instrument calibration, spectroscopic line uncertainty, and physics not included in the operational retrieval code.

Raw and bc XCO2, bias correction variables, and other data are conveniently contained in OCO-2 "Lite" files, with one Lite file per day that includes all daily operational retrievals. Data quality is indicated by Quality Flag=0 (QF0, best quality) and Quality Flag= 1 (QF1, poor quality) data flags. The OCO-2 team discourages use of QF1 data in XCO2 studies. In this paper we do examine QF1 data in addition to the QF0 data since the QF1 data provides insights into 3D cloud radiative effects.

Of the million daily observations which are collected by OCO-2, about 25% are passed into the operational retrieval. Two cloud preprocessors (Taylor et al. 2016) exclude many of the radiances. A quick determination of surface pressure from the O2 A-band is compared to a priori meteorological data. An observation is excluded from the operational retrieval if the difference in surface pressure is greater than 25 hPa. A second quick algorithm compares WCO2 and SCO2 columns. If the ratio of the two columns deviates significantly from unity, then the observation is excluded from the operational retrieval.

Not all known physics, however, is included in the operational retrieval. The OCO-2 operational retrieval does not know if clouds are outside of the row (frame) of the eight side by side detector footprints. The OCO-2 orbital track sweeps out a continuous swath of footprints with a swath width less than 20 km (see Fig. 2.2, OCO-2 L2 ATBD, 2019). Clouds outside of the swath

https://doi.org/10.5194/amt-2022-323
Preprint. Discussion started: 14 December 2022

Atmospheric Measurement Techniques Discussions

can scatter photons into the region of the footprints but the OCO-2 experiment cannot determine the location of clouds outside of the swath.

In this paper we utilize MODIS radiance data at 250 m resolution to study 36 scenes in detail. The 250 m radiances and MODIS cloud mask data is used to specify the locations of clouds in the vicinity of OCO-2 observations. The 36 scenes include 12 ocean glint, 12 land nadir, and 12 land glint scenes. A visual examination of NASA Worldview (https://worldview.earthdata.nasa.gov), and a listing of Lite file latitude, longitude, and QF flags suggested scenes in which several dozen Lite file XCO2 values are present in each scene. Many of the scenes have sun-cloud geometry in which light is reflected off of a cloud feature oriented approximately perpendicular to the incident solar beam (Figure 6 is an example), with clear-sky gaps between the clouds. This geometry is conducive to study 3D cloud effects. For global analyses we use the nearest cloud distance information contained in the dataset associated with a previous paper (Massie et al. 2021) which is available at Zenodo (referred to as "3D metric files", https://doi.org/10.5281/zenodo.4008765). As discussed in Massie et al. (2021), the nearest cloud distance data is based upon an analysis of auxiliary files (Cronk 2018) that contains MODIS 500 m radiances, cloud mask and geolocation information matched to OCO-2 observation geolocation.

Previous studies of 3D radiative transfer (Merrelli et al. 2015) applied the Spherical Harmonics Discrete Ordinate Method (SHDOM) 3D radiative transfer code (Evans 1998) to perturb OCO-2 type spectra, and looked at OCO-2 type retrievals with and without the 3D radiance perturbations. Retrieved XCO2 values were *lower* than clear sky retrievals by 0.3, 3, and 5-6 ppm for surfaces characterized by bare soil, vegetation, and snow-covered footprints.

Massie et al. (2021) calculated differences in XCO2(TCCON) and XCO2(Lite file) for QF0 and QF1 data for several years of OCO-2 measurements. Denoting XCO2(TCCON) – XCO2(Lite file) as Residual(D) at distance D from the nearest cloud, residual differences (Residual(10 km) – Residual(D)) varied between zero and 0.4, and zero and 2.5 ppm, for QF0 and QF1 data as nearest cloud distance D varied from 10 km to 0.5 km. The residuals (with positive values indicating a retrieval *underestimate* of XCO2) are present in both raw and bc XCO2, and therefore are residuals of 3D cloud effects that are not accounted for by the 1D operational retrieval framework.

The recent Emde et al. (2022) study discusses 3D calculations that covers a range of cloud scenes over Germany and surrounding countries, based on a large eddy simulation, and in addition a set of box-clouds with various solar zenith and viewing angles and optical depths. The calculations were carried out in the 400 – 500 nm and O2 A-band spectral ranges. The Figs. in Emde et al. (2022) for the box cloud calculations are particularly instructive as they illustrate how reflectance varies as a function of distance from cloud edges for viewing geometry in which clouds enhance the radiance field and for viewing geometry in which cloud shadow effects are present. The Emde et al. (2022) calculations are available at https://doi.org/10.5281/zenodo.5567616 (Emde, 2021). The study of Emde et al. (2022) motivated us to calculate a set of SHDOM idealized bar cloud 1D and 3D calculations.

This paper is organized in the following manner. The data utilized in our study is discussed in Sect. 2. Details of the SHDOM 1D (IPA, independent pixel approximation) and 3D radiance calculations are reviewed in Sect. 3.1. In Sec. 3.2 SHDOM idealized bar cloud calculations are discussed, which provide insight as to the variation of 1D / 3D intensity ratios as a function of nearest cloud distance, gas vertical optical, solar zenith angle, cloud height, and surface reflectance. Partial derivatives in radiance with respect to changes in pressure, XCO2, reflectance and aerosol total optical depth are presented in graphical form in Sect. 3.3 to illustrate the zero-order physics associated with 3D cloud effects. In Sect. 4 individual scenes over the ocean and

https://doi.org/10.5194/amt-2022-323
Preprint. Discussion started: 14 December 2022

Atmospheric Measurement Techniques Discussions

land are discussed to illustrate how the 1D / 3D radiance intensity ratio varies near and far away from clouds. In Sect. 5 SHDOM calculations for 36 scenes (12 ocean glint, 12 Amazon land nadir, and 12 Amazon land glint) are discussed. The QF0 and QF1 observations illustrate the relationships between nearest cloud distance and key variables (1D / 3D SHDOM radiance intensity ratios, raw XCO2, dP, surface reflectance, and aerosol optical depth). In Sect. 6 yearly calculations of dP and raw XCO2 are presented for 10° latitude bands as a function of nearest cloud distance. Sect. 7 presents our summary and conclusions.

2 Data

OCO-2 product files are available from the NASA Earthdata website (https://earthdata.nasa.gov/) and archived in the GES DISC repository. The first part of specific Version 10 (V10) file path names are given here in parenthesis to identify, in a general sense, the files used in our study. OCO-2 "Lite" files (oco2_LtCO2_..) contain raw and bc XCO2, bias correction variables (such as dP), and other information. The land / water flag is used in our study to identify ocean and land observations, and the operational mode flag is used to identify glint and nadir observations. Preprocessor (oco2_L2ABP_.., referred to as L2ABP files) specify cloud flags and continuum radiances for all measurements (including those which are not successfully retrieved). Level 2 diagnostic files (oco2_L2Dia_..) specify full spectra in all three bands. Meteorological (oco2_L2Met..) surface pressure is specified by GEOS-5 FP-IT data, which is used to calculate the dP values. The ND characters in the granule-level file path names refer to nadir observations, while glint files contain GL as part of the file path name.

Co-analysis of MODIS and OCO-2 data is made possible by way of MODIS 250 m radiances (MYD02QKM..), geolocation (MYD03..), aerosol (MYD04..), cloud data (MYD06..), and weekly surface reflectance (MYD09..). The MY.. prefix indicates MODIS Aqua data files. OCO-2 flies six minutes in front of MODIS Aqua in the NASA "A-train", and therefore the MODIS cloud field in six minutes may differ slightly from the cloud field that impacts OCO-2 observations. The MYD06 data file specifies cloud heights for a given scene. Cloud heights vary between 0.6 and 3.7 km for the scenes examined in this paper, with 1.4 km being the average.

The 3D metric files contain nearest cloud distance and other 3D cloud metrics which are discussed in Massie et al. (2021). The other metrics (H(3D), H(Continuum), and CSNoiseRatio) are based upon calculation of standard deviations of the MODIS radiance field, OCO-2 continuum radiance field, and sub-footprint radiance fields, respectfully. These metrics are measures of *radiance spatial gradients*, which will be non-zero in the presence of clouds. In this paper we focus on nearest cloud distance since Várnai and Marshak (2009) demonstrated that MODIS reflectance at various wavelengths between 0.47 and 2.13 μm increases the closer one is to clouds (i.e. nearest cloud distance is a previously proven 3D cloud effect metric). There are 3D metrics for each successful OCO-2 QF0 and QF1 retrieval for 2014-2019.

3 Calculations

3.1 The SHDOM radiative transfer code

The Spherical Harmonic Discrete Ordinate radiative transfer Method (SHDOM) 3D radiative transfer code (Evans, 1998; Pincus and Evans, 2009) calculates 1D (single column, independent pixel approximation) and 3D fields. In the 1D calculation there is no exchange of photons between

https://doi.org/10.5194/amt-2022-323
Preprint. Discussion started: 14 December 2022

Atmospheric Measurement Techniques Discussions

adjacent columns. In the 3D calculation columns do exchange photons. Of particular interest to our paper is the scattering of photons from cloud and ground to adjacent columns. This exchange of photons between columns yields a 3D Stokes radiation field which differs from the 1D Stokes field. We focus on the total intensity component of the Stokes vector.

Input to SHDOM includes specification of the vertical (z-axis) gas optical depth structure, and the x-y-z mass content structure of the cloud and aerosol fields. In our calculations the horizontal x-y grid has a grid spacing of 0.5 km, and the input gas files have a 1 km grid spacing from ground to 30 km altitude. The number of x and y axis grid points is 64, so the full SHDOM x-y grid covers a 32 km by 32 km area. Since the cloud and aerosol input file has an altitude grid at sub-1 km spacing near the ground, SHDOM interpolates the gas field extinction / km values to the sub-1km vertical grid of the cloud and aerosol input file. Gas field extinction / km values are calculated by utilizing the OCO-2 ABSCO data files (Payne et al, 2020). The ABSCO molecular cross sections for O_2, CO_2, and H_2O, specified at a resolution of 0.010 cm^{-1} (5.9 10^{-7} μm in the O2 A-band), are tabulated as a function of 64 pressures and 17 temperatures. Extinction / km values are calculated for each x-y-z grid point according to each grid point temperature and pressure. A constant Lambertian surface reflectance in each band for land observations is chosen to bring the SHDOM 3D top of atmosphere reflectance in agreement with the observed reflectance. For ocean glint observations the Mishchenko and Travis (1997) implementation of the Cox-Munk windspeed dependent surface reflectance formulation is used in the SHDOM calculations, with windspeed specified from Lite file data.

For a specified wavelength, SHDOM calculates Rayleigh scattering, aerosol, and cloud optical parameters (optical depth, asymmetry parameter, and single scattering albedo) for each x-y-z grid cell. For the scenes discussed in this paper the aerosol and cloud radii are 0.1 and 10 μm, respectively. Water droplet clouds have a cloud base of 0.1 km to a specified cloud height (e.g 1.4 km), with a constant cloud droplet liquid water content (LWC, in g /m^3 units). The aerosol has equal valued extinction / km values from ground level to 1.8 km altitude The input aerosol mass content values are adjusted such that the total vertical aerosol optical depth is near a desired value (in the 0.05 - 0.16 range, and usually less than 0.1). Since the aerosol optical depth is small, surface reflectance should have more influence on the top of atmosphere radiance than aerosol. SHDOM calculates the aerosol and cloud optical depth parameters by applying a Mie code based on the input cloud and aerosol file, and for aerosol the complex index of refraction is selected based on a sulfate aerosol.

SHOM is configured to write out the Stokes field at the top of the atmospheric grid for a set of sun-observation azimuth angles, solar zenith angle, sensor view angle, for 17 total vertical gas optical depths. For the O2 A-band the gas optical depths vary from 8 10^{-4} to 4.0. The lowest gas optical depth in each band corresponds to the band continuum.

The observed radiances are directly related to the SHDOM 3D radiances, since actual atmospheric radiances are the result of 3D radiative transfer processes. The 1D radiance field is not available from OCO-2 measurements, though the 3D radiances approach the 1D values as cloud distances become very large. Also, the OCO-2 radiances are dependent upon a linear combination of the I, Q, and U Stokes components (see equation 3-40, OCO-2 L2 ATBD, 2020). We focus on the SHDOM total intensities to gain insights in regard to 3D cloud effects for a variety of scenes, and do not make detailed comparisons of observed spectra and the SHDOM spectra.

https://doi.org/10.5194/amt-2022-323
Preprint. Discussion started: 14 December 2022

Atmospheric Measurement Techniques Discussions

3.2 Idealized bar cloud calculations

The choice of idealized bar cloud calculations is motivated by visual examination of various NASA Worldview scenes over the ocean and the Amazon. Amazon clouds are frequently distributed in "cloud streets" (Fig. 6 is a good example). Ocean scenes, in which an elongated cloudy area is associated with adjacent clear sky regions, are useful to study 3D cloud effects (Fig. 8 is a good example). The cloud distributions in both scenes can be geometrically approximated by one or more idealized bar clouds.

Figure 1 illustrates a pair of idealized bar clouds, referred to as *left* and *right* bar clouds. The x width of each cloud is 3 km, and the bar clouds extend the full y-axis of the 32 km by 32 km scene. The clouds are assigned a specific solar zenith angle and cloud altitude (1.4 km). The sun is along the x-axis and SHDOM is configured to calculate for 12 sensor azimuth angles from 0 to 360° in 30° steps. Figure 1 illustrates one of the 12 azimuth angles, with the sensor to the right of the right bar cloud. The inclusion of the two clouds in the scene allows for analysis of 1D and 3D radiances that result from scattering of photons off the right bar cloud back towards the observation footprint (Obs), and for the case in which (for the left bar cloud) a cloud shadowing effect is present if the observation point is close to the left bar cloud. The spatial extent of the cloud shadowing is dependent on the height of the cloud and the solar zenith angle. Analysis of the 1D and 3D radiances as a function of distance D from the bar clouds yields insights into the nature of 3D radiative effects, as a function of gas vertical optical depth.

The 1D / 3D ratio, and its variation in a scene, is fundamental to this paper, since it is a measure of the size of the 3D cloud effect in the scene. Figure 2 presents 1D / 3D ratios as a function of cloud distance D from the right bar cloud for all three OCO-2 bands. Land nadir geometry is applied, with a solar zenith angle of 38° (with atmospheric model specifics associated with the Amazon scene discussed in Fig. 6 below). The curves pertain to a low gas vertical optical depth near 0.01. The 1 D / 3D ratios approach unity as the cloud distance increases. The ratios for the optically thin regime however are not equal to 1.0 at the largest cloud distance since photon paths are present in the 3D case in which light propagates into the top of the cloud and exits out the sides, adding to the 3D radiances in the regions between the clouds. As the cloud distance D decreases towards zero the 1D / 3D ratio becomes small, near 0.3. Notice that this drop off in the ratio is very non-linear, and takes place at cloud distances approximately less than 4 km. Also notice that the curves for the three bands are quantitatively different. This implies that a detailed understanding of 3D radiative effects requires attention to the details in each of the three OCO-2 bands.

Figure 3 displays 1D / 3D ratios as a function of cloud distance D for the left and right bar clouds for the O2 A-band continuum (gas optical depth near 0.008). For the left bar cloud the ratio decreases as cloud distance decreases from large values, then increases as distance D approaches zero. This behavior is due to *cloud shadowing* effects. For graphical convenience the 1D / 3D ratio is set to a maximum value of 1.2. The 1D radiance is not susceptible to cloud shadowing since the cloud shadow originates from the sunward-adjacent column. The 3D radiance is susceptible to the shadowing from the adjacent column. 3D radiance fields are therefore susceptible to both cloud shadowing (dimming) and cloud brightening effects. The prevalence of cloud brightening versus cloud shadowing effects is discussed in Section 4.

Figure 4 indicates the sensitivity of 1D / 3D ratios to gas vertical optical depth, solar zenith angle, cloud height (cloud vertical extent), and surface reflectance. The curves are those from idealized bar cloud calculations for the right bar cloud. The largest sensitivity is due to the gas optical depth. The sensitivity is largest for the smaller nearest cloud distances. As the gas optical

https://doi.org/10.5194/amt-2022-323
Preprint. Discussion started: 14 December 2022

Atmospheric Measurement Techniques Discussions

depth increases the ratios become closer to unity, and the curves drop-off to lower ratios at increasingly smaller cloud distances. For the case where optical depths become very large the ratio approaches unity for all cloud distances. This is reasonable since at very large gas optical depths the vast majority of the photon paths are located at large heights above the surface, and these photons do not interact with the low-level clouds.

The second largest sensitivities are due to solar zenith angle and cloud height. The sensitivity to solar zenith angle is reasonable since for larger solar zenith angles photons are scattered off of the sides of the clouds, while for a solar zenith angle near zero the 3D radiative effect is constrained by photon paths passing through the top of the cloud (followed by some exiting of photons to the side) and/or secondary paths (sun to surface, surface to cloud, cloud back to surface).

In the lower left panel of Fig. 4 the sensitivity to cloud thickness is illustrated (labeled by the cloud top height) for a cloud base of 0.1 km. As the vertical extent of the cloud is increased there is more side surface area present, increasing the number of sun to cloud to surface photon events. As noted by Taylor et al. (2016), the cloud preprocessor does a good job in screening for clouds, though the preprocessor can pass some cases in which low-level clouds are present.

The lower right panel of Fig. 4 indicates that 1D / 3D ratios are not sensitive to surface reflectance for the land nadir view geometry. Since the 1D path (sun to surface to sensor) is dependent on the surface reflectance, and the 3D situation (with added sun to cloud to surface to sensor paths) is also dependent on the surface reflectance, some cancellation in the surface reflectance term is expected.

3.3 Radiance perturbation sensitivity

Figure 5 illustrates the sensitivity of radiances to perturbations in XCO2, surface pressure, surface reflectance, and total optical depth. The x axis variable specifies the total vertical optical depth (gas + aerosol) for each band, while the y axis variable specifies the radiance perturbation. Denoting R as the radiance intensity, the 3D curves in each panel are 100 (R(3D) – R(1D)) / R(1D) values, where 3D and 1D refer to SHDOM 3D and 1D calculations. The observation point (see Fig. 1) is 4 km leftward of the right bar cloud, with the sun (sensor) to the left (right) of the observation point. The other curves are partial derivatives of the 1D radiances, 100 (R(1D perturbation case) – R(1D baseline case)) / R(1D baseline case). Baseline conditions and perturbations are specified in Table 1. The solar zenith and sensor view angles are 38° and 0°, respectively, in all of the calculations. The atmospheric profile corresponds to the Amazon scene associated with Fig. 6 that is discussed in section 4. Sulfate aerosol extends from ground to 1.8 km, with a total optical depth near 0.064 in the O_2 A-band, cloud LWC is 0.30 g / m^3, and the idealized bar clouds have a cloud top at 1.4 km.

Figure 5 illustrates that an *increase* in radiance comes about (in a partial derivative sense, with other variables held constant) if surface reflectance or aerosol optical depth is *increased*, if the surface pressure is *decreased*, or if XCO2 is *decreased* in the WCO2 and SCO2 bands. *Away from clouds (in the absence of radiance dimming due to cloud shadows), the 3D effect increases radiance.* Since the 3D effect is substantial at all optical depths, it is expected that the retrieval will definitely adjust surface reflectivity and/or aerosol in the state vector, since these variables have radiance partial derivatives that are also non-zero at all optical depths. The surface pressure perturbations in all three bands, and the WCO2 and SCO2 XCO2 perturbations, have radiance partial derivatives that are small at small gas optical depths, and appreciable only at the larger vertical optical depths. Figure 5 does not indicate how the 3D radiance perturbation is accounted

https://doi.org/10.5194/amt-2022-323
Preprint. Discussion started: 14 December 2022


Atmospheric Measurement Techniques Discussions

for in the operational retrieval by perturbations in surface reflectance, aerosol, surface pressure, and XCO2. This question is addressed below in section 5.

Figure 5 illustrates that OCO-2 observations are susceptible to 3D cloud effects. The 3D effect is present in all three bands, increasing 1D radiances from 2 to 4% when the observation point is 4 km from the right bar cloud. The spectral variations of the 3D radiance perturbations in Fig. 5 are distinct (different than the other perturbations), which forces adjustments in the retrieval state vector variables. The 3D perturbations are larger (smaller) for smaller (larger) cloud distances. As stated in the Introduction, the OCO-2 measurement goal is to measure XCO2 to the 1 ppm level. Perturbations in XCO2 of 1 ppm, however, perturb radiances on the 1 % level only at large optical depths, and less so at smaller optical depths. If the 3D radiance perturbations were substantially smaller than the radiance perturbation corresponding to a 1 ppm increase in XCO2, and if the spectral variations of the 3D radiance perturbations were not different than the other perturbations, then the OCO-2 observations would not be susceptible to 3D cloud effects, but this is not the case. Since 40% of all OCO-2 observations are within 4 km of clouds, 3D cloud radiative effects impact many OCO-2 observations (Massie et al. 2021).

Fig. 5 illustrates the zero-order physics associated with 3D radiative transfer. The discussion then needs to proceed to ask how the operational retrieval responds to the 3D radiance enhancements due to 3D cloud brightening effects. Since the operational retrieval does not insert any 3D radiative transfer physics into the retrieval, there is a needed adjustment of state vector element values to bring forward model and observed radiances in agreement. The operational retrieval obtains a solution state vector with specified surface pressure, surface reflectivity, aerosol, and XCO2 which brings forward model radiances in line with observed radiances. There is no reason to assume that only the surface pressure, surface reflectivity, and aerosol state vector elements provide for the needed radiance enhancement due to 3D cloud radiance brightening, with XCO2 not also providing for the needed radiance enhancement.

4 Amazon and Ocean Glint scenes

Figure 6 presents the detailed SHDOM calculation for a scene over the Amazon on June 22, 2015. The direction of the incident sunbeam is from the northwest at the solar zenith angle of 38°, while the nadir view (OCO-2 sensor view) angle is 0°. The altitude, pressure, and temperature model atmosphere is derived from the oco2_L2MetND file, with specifics listed in Table 1. Clouds are specified by analysis of the MODIS MYD02QKM 250 m radiance, MYD03 geolocation, and MYD06 cloud fields. The MYD06 cloud field identifies some clouds, and these clouds are used in conjunction with the MYD02QKM radiances to establish a cloud radiance threshold. The MYD06 cloud field, however, does not identify all clouds in a scene. This is apparent by examining the MODIS 250 m radiance field and the MYD06 cloud field (Massie et al. 2017). Once the cloud radiance threshold is established from examination of the MODIS radiance field, clouds are assigned to all x-y grid points if the MODIS radiance is greater than the threshold value. In Fig. 6 clouds are present when the radiance is greater than 80 $W/m^2/sr/\mu m$.

Note that the locations of the Lite V10 file data points are *between the clouds* and are indicated by the square □ and X symbols for the QF0 and QF1 retrievals. The cloud preprocessor does a good job in screening for observations over clouds and/or the operational retrieval does not converge successfully for these data points.

Table 2 (first column) presents statistics for the latitude range 10° S to 3° N on June 22, 2015, which includes many more data points that those displayed in Fig. 6. Of 5162 OCO-2 observations,

https://doi.org/10.5194/amt-2022-323
Preprint. Discussion started: 14 December 2022


Atmospheric Measurement Techniques Discussions

589 observations (0.11 in fractional terms) were successfully retrieved, with 0.40 and 0.60 QF0 and QF1 retrievals, respectively. Approximately 0.80 of the retrievals are located within 4 km of clouds.

The prevalence of cloud brightening versus cloud shadowing effects for the Amazon scene is revealed in Table 2. Table 2 specifies the fraction of total retrievals which are associated with cloud shadows, assuming that the cloud heights are 2, 4, 6, or 8 km. The fractions for each cloud height are calculated based on the following algorithm, described in the following three paragraphs. The algorithm utilizes O2ABP preprocessor cloud flags to identify clouds and clear observations and OCO-2 Level 1B data files that specify O_2 A-band continuum radiances. The continuum radiances and cloud flags are used together to specify clear and cloudy radiance thresholds. Details of the algorithm are discussed since the calculation is nontrivial.

Using the Amazon observations on June 22, 2015 (150622) as an example, the L2ABP preprocessor data file specifies the cloud flag (0=clear, 1=cloudy, 2=undetermined) and O2 A-band continuum radiances for each OCO-2 measurement are specified by the OCO-2 Level 1B data files. Average clear and cloudy continuum radiances (Clear(bin) and Cloudy(bin)) are determined in 0.5 latitude bin steps for the 10 S to 3 N latitude range. It is necessary to consider two dozen latitude bins since some bins are fully cloudy, and some bins have relatively few clouds. A Clear(ave) radiance average is calculated from the Clear(bin) averages when the fraction of clear flags for a latitude bin is greater than 50%. A similar calculation is done for the Cloudy(ave) average. Guided by SHDOM calculations, for bar clouds similar to Fig. 1, with cloud tops at 2, 4, 6, and 8 km, the 3D radiances are analyzed to determine an average observation to cloud radiance ratio Ratio(obs, cloud), with Ratio(obs, cloud) determined from 3D radiance (distance D from the cloud) / SHDOM 3D radiance (position located over the cloud) ratios. These calculations yield a SHDOM threshold Ratio(threshold) near 0.30. Since there is a range of Cloudy(bin) values for the various latitude bins on an individual day, Ratio(threshold) is conservatively increased to 0.60 (which will overestimate the cloud shadow "Fraction Geom" values in Table 2).

For a specific observation point, L2ABP locations surrounding the observation point are examined. A 10 km by 10 km box surrounds the observation point, and the algorithm loops over L2ABP data file longitude I, latitude J indices. Ratio(obs; I,J point) values, equal to the O2 A-band L2ABP radiance(obs point) divided by the O2 A-band L2ABP radiance(I, J point), are calculated. The distances Distance(obs; I,J point) from the observation point to the I, J positions are calculated. The angles Angles(obs; I, J point) between the fixed solar vector (observation point to Sun location) and geometry vectors (from the observation point to the L2ABP I, J positions) are also calculated. For a given cloud height (e.g. 4 km), the solar zenith angle and cloud height determines the Xshadow(km) spatial length that the shadow corresponds to.

In general, if a) the positions of the sun, L2ABP file I, J position, and observation point are in a line with the I, J point in the middle of the line, if b) Distance(obs, I, J point) is less than Xshadow(km), if c) Ratio(obs; I, J point) is less than Ratio(threshold), if d) the I, J point has a L2ABP cloud flag equal to 1 (cloudy case), and if e) Angles(obs; I,J point) is less than a threshold angle difference (e.g. 30°), then the observation point is associated with a shadow. The code-wise loops check to see if a shadow is associated with each observation point, and then calculates the fraction of retrievals that are associated with shadows for each cloud height.

Of the 589 successful retrievals for the Table 2 Amazon 150622 case, only eight retrievals (0.013 in fractional terms) are associated with shadows, assuming that all cloud heights are 8 km in vertical extent. The fractions are less for lower cloud heights. The additional columns of Table 2 indicate that the Pacific Glint observations (the June 12, 2016 (160622) case, discussed below),

https://doi.org/10.5194/amt-2022-323
Preprint. Discussion started: 14 December 2022

Atmospheric Measurement Techniques Discussions

and yearly averaged fractions over the Amazon and Pacific in 2016 are less than 4%, even if all cloud heights are 8 km. Cloud heights, however, are less than 8 km. Application of NASA Giovanni (https://giovanni.gsfc.nasa.gov/giovanni/) analysis of MODIS MYD08 data files yields histograms (not shown) of cloud top temperatures and pressure means which correspond to cloud top heights between 1 and 2 km for the 150622 and 160622 cases, and heights between 2 and 3 km for the 2016 Amazon and Pacific yearly averages. *Cloud brightening therefore is prevalent compared to cloud shadowing.*

Figure 7 presents the SHDOM calculation of 1D / 3D ratios for the Fig. 6 Amazon scene for a gas vertical optical depth of 0.0008 (an optical depth in the O2 A-band continuum). The V10 Lite file data points have 1D / 3D ratios in the 0.47 – 0.96 range, with an average of 0.91. *Successful OCO-2 retrievals are therefore susceptible to significant 3D cloud radiative perturbations on the order of 9 %.* The darkest areas have 1D / 3D ratios dipping down towards 0.3, and are located on the sunward side (northwest side) of the clouds, since the sunbeam direction is from the northwest.

Figure 8 presents a glint scene at 10° N on June 12, 2016 over the Pacific with a solar zenith angle of 24° and sensor view angle of 19°. Square □ and X symbols mark the locations of the Lite file QF0 and QF1 retrievals in the MODIS radiance field. The date is near the summer solstice and the sun beam direction is from the northwest. More QF0 data (the square symbols) are located to the south of the cloud in the center of the frame, with fewer square symbols on the sun-reflective side of the cloud (the region northwest of the cloud). This indicates that cloud brightening regions (northwest of the clouds) are more likely to generate QF1 data points than cloud dimming regions (southeast of the clouds).

Figure 9 presents the SHDOM 1D / 3D ratios for this oceanic scene. Figure 9 and Fig. 6 are similar in that the smallest 1D /3D ratios are located close to clouds. The ratios however are not equal to unity for the continuum wavelength (smallest total optical depth), and are near 0.94 at x=13 km and y = 22 km, and near 0.97 at y values north of this point in Fig. 9. *This indicates that 3D cloud effects can "reach" several kilometers away from clouds.*

5 Analysis of multiple scenes

Lite file variables and SHDOM 1D and 3D radiance fields are analyzed for 36 individual scenes (12 ocean glint, 12 land nadir, and 12 land glint geometry). The specifics for the scenes are given in Table 3. A range of solar zenith angle from 20° to 55° characterizes the ocean glint scenes. The land scenes are situated over the Amazon. It is of interest to study Amazon scenes since there are relatively few successful QF0 data points over the Amazon, and the Amazon is of large importance to the global carbon cycle. The majority of completed retrievals over the Amazon are QF1 retrievals. Several Amazon scenes were chosen purposely to make sure that there were at least some QF0 data points in the scenes.

Figure 10 presents individual sun glint retrievals over the Pacific. QF0 and QF1 data points are given by the green (*) and blue (+) symbols. In the upper left panel SHDOM 1D / 3D ratios for continuum O2 A-band (for the smallest gas optical depth) and 3D metric file nearest cloud distances are graphed. The 1D / 3D ratios are near unity for cloud distances greater than 4 km. The ratios become smaller, with smallest values near 0.3, as the nearest cloud distance approaches zero. The largest number of QF0 data points are for large cloud distances, while the largest number of QF1 data points are for small cloud distances.

In the bias correction processing step, a specified limited range for 23 variables determines if a retrieval is a QF0 data point (see Appendix A of O'Dell et al. 2018 for the Version 8 data files).

https://doi.org/10.5194/amt-2022-323
Preprint. Discussion started: 14 December 2022

Atmospheric Measurement Techniques Discussions

As an example, a retrieval is a QF0 data point if dP is between -4 and 10 hPa for ocean observations and -6 and 14 for land observations for the Version 8 data files.

In the upper right panel of Fig. 10 the dP values for QF1 data points take on large negative values as cloud distance approaches zero. The interpretation of the upper two panels is that the 1D / 3D ratio becomes small as the 3D cloud effect enhances (brightens) the radiances. In order for the retrieval to match the forward model with the observed radiance, the retrieval decreases the surface pressure to smaller values (compared to the meteorological surface pressure field), and increases aerosol optical depth, at small nearest cloud distance.

To place the various scene XCO2 values onto a common framework, we calculate the average QF0 XCO2 for a 6° range of latitude centered on the scene's latitude. The average is then subtracted from the QF0 and QF1 raw XCO2 for a specific scene, and these adjusted raw XCO2 values are placed into our graphs. In the middle-left panel of Fig. 10 the adjusted raw XCO2 varies from – 2 to 2 ppm for the QF0 data at all nearest cloud distances. For the QF1 adjusted raw XCO2 data the values take on increasingly negative values as nearest cloud distance decreases. *The concurrent decrease in the 1D /3D ratios and raw XCO2, as nearest cloud distance decreases, is evidence of 3D cloud effects in the OCO-2 retrievals, especially for the QF=1 observations.*

The middle-right panel of Fig. 10 displays total aerosol optical depth, which takes on increasingly larger values as nearest cloud distance decreases for the QF1 data. The fractions of QF0 and QF1 data points at cloud distances less than 4 km are 51% and 86% of the total number of QF0 and QF1 data points, respectively. Since each scene has a different inherent aerosol optical depth, it is expected that there will be several green (*) sets of data points (the rightward directed spikes of total aerosol optical depth in the middle-right panel).

In the V10 retrieval surface reflectance is represented by the sum of Cox-Munk surface glint and Lambertian surface terms. The lower left panel displays the retrieved O2 A-band Lambertian surface reflectance (Albedo1) values *added* to the Cox-Munk term. (The V10 Lite files do not specify the total surface reflectance values over the ocean, while the files do specify the total surface reflectance over land). The lower right panel displays "delta Wind" values (the difference in retrieved wind speed and a priori wind speed, in m units). Since an increase in wind speed generally leads to a smaller surface reflectance, the positive delta Wind and Albedo1 values for QF=1 data indicate that the retrieval selects decreasing Cox-Munk and increasing Lambertian contributions to the total surface reflectance as nearest cloud distance varies from large to small values.

Figure 11 displays panels for the Amazon land nadir scenes. The behavior of the data points is similar to the ocean glint data, though the range of nearest cloud distance is smaller than for the ocean glint scenes. Since the selected ocean and Amazon scenes were picked in a purposeful manner, this range difference is not generally true (see the next section for yearly analyses). The 1D / 3D ratios in Fig. 11, however, do decrease as the cloud distance decreases in the upper left panel. As cloud distance decreases the adjusted XCO2 values take on increasingly negative values in the middle-left panel. The range in QF1 XCO2 for cloud distances greater than 5 km is larger for the Amazon land nadir scenes. Standard deviations for ocean glint XCO2 are generally smaller than land XCO2 (see Fig. 18 of O'Dell et al. 2018 and Table 4 of Massie et al. 2021). The fractions of QF0 and QF1 data points at cloud distances less than 4 km are 74% and 84% of the total number of QF0 and QF1 data points, respectively.

From Fig. 5 and Table 1a change in 0.02 and 0.01 in O2 A-band and WCO2 surface reflectance yields an increase in radiance which is *twice* as large as the 3D radiance perturbation, so small changes in the QF0 and QF1 surface reflectance values (referred to as "albedo" values in the Lite

https://doi.org/10.5194/amt-2022-323
Preprint. Discussion started: 14 December 2022


Atmospheric Measurement Techniques Discussions

files and in Figs. 11 and 12) are amply sufficient to "add sufficient 3D radiance" to bring forward model and observed radiances into agreement. There is a noticeable difference in Figs. 10 and 11 in that the ocean glint scenes have dP less than -10 hPa for the QF1 data, while there are few dP values less than -10 hPa in Fig. 11 for the land nadir scenes.

Figure 12 displays land glint data. The 3D metric files have nearest cloud distance data for four of the 12 land glint scenes (the LG 150625 scenes, as specified in Table 3). Nearest cloud distance values for the LG 200603 and LG 200610 scenes of Table 3 were calculated based on Lite file longitude and latitudes and 250 m MODIS radiance fields. SHDOM 1D / 3D ratios and raw XCO2 decrease as cloud distance decreases, while total aerosol optical depth increases, especially for the QF1 data. In contrast to Fig. 11, the retrieval selects O2 A-band and WCO2 band surface reflectivity at small cloud distances for some (~ dozen) of the data points, which are smaller than the surface reflectivity at large cloud distance.

6 Yearly analysis

Generalization in differences in ocean glint, land nadir, and land glint are best made from an analysis of yearly averaged data using the daily Lite file and 3D metric files for each full year of OCO-2 data during 2015-2018. Since the 3D metric files do not include 1D / 3D SHDOM ratios, which are only available for the 36 scenes discussed above, the nearest cloud distance is the primary 3D metric utilized in this section.

The nearest cloud distance averages for 2016 are presented in Figure 13. *It is apparent that clouds are closer on average for OCO-2 observations over the ocean than over land*. This is especially true for the QF1 data which is approximately 4 km from clouds over the ocean. The 4 km mark is important since the curves in Figs. 2 - 4 become very non-linear at distances near and below 4 km cloud distance. The cloud distance is noticeably smaller over the equator over both land and ocean, with a symmetrical appearance with respect to the northern and southern hemispheres.

Averages of dP for several 10° latitude bins in the tropics are displayed in Fig. 14. The QF1 ocean glint curves are best defined, with large negative dP values at cloud distances less than 5 km, and dP between -1 and 1 hPa for cloud distances greater than 5 km. This signature is evidence of 3D cloud effects that impact the OCO-2 radiances. The data points in the upper right panel of Fig. 10 are consistent with the Fig. 14 dP tropical averages. The land nadir and land glint dP curves in the tropics, however, increase in dP by several hPa as cloud distance decreases, with dP values in the positive 0 to 4 hPa range.

Averages (denoted as Ave) of raw XCO2 for the same tropical latitude bins in Fig. 14 are displayed in Fig. 15. The QF1 XCO2 curves are again best defined for the ocean glint curves, with fewer oscillations in the curves than for those over land. Raw XCO2 decreases by 0.3 to 0.7 ppm as the cloud distance decreases in the tropics for the QF0 data, and decreases by 1.2 to 2.3 ppm for the QF1 data. *Since the 3D cloud-retrieval bias is given by the difference Ave(20 km) – Ave (0 km), the 3D cloud-retrieval biases for QF0 and QF1 data are between 0.3 and 0.7 ppm, and between 1.2 to 2.3 ppm, respectively, in the tropics.* (The *3D cloud-retrieval bias* is the raw XCO2 bias introduced by the retrieval, and does not refer to the retrieval of cloud properties). The Fig. 14 and Fig. 15 average curves indicate that the operational retrieval *underestimates* XCO2. The raw XCO2 land nadir and land glint averages for QF0 data decreases by 0.3 to 0.6 ppm as cloud distance decreases, and by 1.5 to 3.0 ppm for the QF1 data.

https://doi.org/10.5194/amt-2022-323
Preprint. Discussion started: 14 December 2022

Atmospheric Measurement Techniques Discussions

A visual examination of the graphs (not shown) of the average dP and raw XCO2 curves for 2015, 2017, and 2018 display many similar qualitative features to those displayed by the 2016 Figs. 14 and 15 curves. While XCO2 has increased during 2015 – 2018 (by approximately 2 ppm per year), the shapes of the curves are qualitatively similar year to year.

Figure 16 displays ΔdP averages (i.e. dP (near 20 km) – dP (near 0 km) differences) as a function of latitude for 2015 – 2018 as a function of nearest cloud distance. Instead of just using the raw XCO2 values at 20 and 0 km cloud distance, averages for 18-21 km and 0-3 km are calculated to bring more data into the averaging process. The ocean glint QF0 ΔdP averages are slightly positive at all latitudes. The ocean glint QF1 ΔdP averages are consistently positive at all latitudes, with values between 2 and 4 hPa for latitudes southward of 30° N. There is a hemispherical asymmetry in the ΔdP land values, with negative ΔdP QF1 values near -4 hPa at 20° S and values near zero in the northern hemisphere. The reason for this asymmetry is not known.

Figure 17 displays ΔrawXCO2 averages (i.e. raw XCO2 (near 20 km) – raw XCO2 (near 0 km) differences) as a function of latitude for 2015 – 2018 as a function of nearest cloud distance. The ΔrawXCO2 averages are an appropriate measure of 3D cloud-retrieval biases (in ppm units) that are present in OCO-2 data files. Table 4 specifies the range of these biases for the six lines in Fig. 17. The ocean glint QF1 ΔrawXCO2 biases are consistently above 1 ppm, with a latitudinal average near 1.5 ppm.. *This indicates that ocean glint QF1 data is underestimated by an amount roughly equal to the 1 ppm OCO-2 measurement goal*. The ocean glint QF0 data has an average ΔrawXCO2 near 0.4 ppm. Land glint and land nadir QF1 average ΔrawXCO2 is positive in the northern and southern hemispheres, while the QF0 average ΔrawXCO2 is positive (0.25 ppm) in the southern hemisphere and negative (-0.25 ppm) in the northern hemisphere. This asymmetry is likely related to the ΔdP hemispherical asymmetry present in the Fig. 16 curves.

7 Conclusions

The OCO-2 cloud preprocessor does a very good job in screening observations near and over clouds. The preprocessor, however, does not necessarily toss out observations that are located between clouds. Figs. 6 and 8 illustrate typical scenes over land and ocean in which successful OCO-2 retrievals are located away from clouds, with QF1 data usually closer to clouds than the QF0 data. The clear sky observations are of most importance in regard to 3D cloud effects since there are few successful QF=0 retrievals over and closely adjacent to clouds.

Since clouds can both add photons to the OCO-2 sensed footprint radiance (when photons bounce laterally off nearby clouds, brightening the surrounding region) or generate a shadowing effect (due to sun to cloud to footprint shadowing geometry), the effect of 3D clouds on OCO-2 retrievals is expected to impose negative and positive radiance perturbations. But cloud brightening events are prevalent compared to cloud shadowing events. Yearly analysis of Amazon and Pacific regions (Table 2) yields retrieval fractions associated with cloud shadowing to be less than 4% for cloud heights less than or equal to 8 km. The unequal fraction of cloud brightening (96%) versus the cloud shadowing (4%) fraction in the retrieved observations imposes an asymmetry in the imposed 1D / 3D intensity ratio radiance perturbations, with fewer cloud shadowing ratios greater than unity, compared to cloud brightening events with ratios less than unity.

The fact that cloud brightening dominates in Fig. 10, compared to cloud shadowing, has important implications for the Fig. 10 OCO-2 retrievals. From Fig. 3 (right panel) cloud shadows are associated with SHDOM 1D / 3D ratios greater than unity. The upper left panel of Fig. 10 has

https://doi.org/10.5194/amt-2022-323
Preprint. Discussion started: 14 December 2022

Atmospheric Measurement Techniques Discussions

observed Lite file retrievals over the ocean with SHDOM 1D / 3D ratios decreasing to low values as nearest cloud distance decreases, with little evidence of ratios greater than unity. The 1D / 3D intensity ratio averages are 0.94 and 0.89 for the QF=0 and QF=1 data points. The radiance brightening is associated with retrieval dP (retrieved – meteorological field) values less than zero, with a sharp decrease in dP for small cloud distances. The upper left and right panels, and middle left panel of Fig. 10, is consistent with the presence of 3D cloud effects in OCO-2 data, since SHDOM 1D /3D ratios, retrieval dP, and raw XCO2 decreases as nearest cloud distance decreases. The cloud brightening is accounted for by the retrieval by a combination of increased aerosol optical depth (middle right panel), decreases in dP, and decreased XCO2, as nearest cloud distance decreases. This is most apparent in the QF=1 data points in Fig. 10. This is also illustrated by Figure 11 of Massie et al (2021), for a larger set of data points.

3D cloud effects in ocean glint, Amazon nadir, and Amazon glint observations are evident in Figs. 10, 11, and 12 since 1D /3D ratios and raw XCO2 concurrently decrease as nearest cloud distance decreases, especially for the QF=1 data points. Using Fig. 5 as a rough guide, an increase in aerosol, an increase in surface reflectance, and decreases in surface pressure and XCO2, yield positive radiance perturbations. There are differences over ocean and land retrievals in that dP variations are smaller over land (compared to the large decrease in dP for the ocean glint retrievals, upper right panel in Fig. 10), and that there are some retrievals for land glint observations in which decreases in surface reflectance are present as nearest cloud distance decreases. There is commonality in Figs. 10, 11, and 12 in that the y-axis spread in dP, XCO2, aerosol, and "delta Wind" is largest as nearest cloud distance decreases.

Since only a limited number of scenes (12 ocean glint, 12 land nadir, 12 land glint) are studied in section 5, yearly average dP and raw XCO2 curves are calculated and presented in section 6. These average curves, displayed in Fig. 15, indicate that the operational retrieval *underestimates* the tropical (10° S to 10° N) raw XCO2 by 0.3 to 0.7 ppm, and by 1.2 to 2.3 ppm, due to 3D cloud effects for the QF0 and QF1 data, respectively.

Figures 15 and 16 display ΔrawXCO2 (i.e. dp(near 20 km) – dp(near 0 km) differences) and ΔrawXCO2 (i.e. raw XCO2 (near 20 km) – raw XCO2 (near 0 km) differences) for 2015 – 2018 as a function of latitude. The QF1 ocean glint averages are the clearest evidence of 3D cloud effects. The ΔdP and ΔrawXCO2 3D cloud-retrieval biases take on increasingly negative values as nearest cloud distance decreases, while the dP values are in the – 1 to 1 hPa range in Fig. 14 at large cloud distance. 3D cloud effects are expected to asymptote to zero as the cloud distance becomes very large. Table 4 specifies averages of the Figure 17 curves. The ocean glint QF0 (QF1) latitude average ΔrawXCO2 biases are near 0.4 (1.5) ppm, while land nadir and land glint biases are near 0.25 and -0.25 ppm for QF0 data in the southern and northern hemispheres.

While 1D radiative transfer theory is extensively covered in papers and textbooks, 3D radiative transfer "rule of thumb" knowledge is not well established. The calculation of idealized bar clouds provides insight as to how 1D / 3D ratios vary as a function of 3D cloud metrics. Of the various possible cloud metrics to consider, nearest cloud distance readily comes to mind since the 3D cloud effect obviously becomes small if clouds are far away from observation points. The systematic variation in 1D / 3D ratios can be discerned by applying the Fig. 1 geometry. Figure 2 indicates that the 1D / 3D ratio is closest to unity far away from clouds, and decreases towards smaller values as cloud distance D decreases, and that the O2 A-band will likely have the largest 3D cloud effect, followed by the WCO2 and SCO2 bands.

The Fig. 4 curves from idealized bar cloud SHDOM calculations are presented to convey insights into the factors which *modulate* 3D cloud effects. Fig. 4 indicates the sensitivity of 1D /

https://doi.org/10.5194/amt-2022-323
Preprint. Discussion started: 14 December 2022

Atmospheric Measurement Techniques Discussions

3D ratios as a function of vertical gas optical depth, solar zenith angle, cloud top height (cloud vertical extent), and surface reflectance. The sensitivity is largest for the smallest vertical gas optical depths since photon paths for the largest optical depths do not sample the lower altitudes. Sensitivity to solar zenith angle is expected since lateral scattering of photons off of cloud surfaces is dependent on viewing geometry.

Figure 2 also indicates that the 1D / 3D ratios are appreciable in size. With 80 % of the Amazon retrievals within 4 km of clouds (Table 2), 1D / 3D ratios are less than 0.95. While the 1D operational retrieval does not take into account 3D nearest cloud distance information, or other 3D metrics, 3D cloud brightening effects, however, are indirectly accounted for in the post-retrieval bias correction process by the dP variable (the difference in retrieved and meteorological data). Figure 5 and Table 1 indicate that small changes in O2 A-band and WCO2 surface reflectance, on the order of 0.02 and 0.01, respectively, yield an increase in radiance *twice* as large as the 3D radiance perturbations illustrated in Fig. 5.

3D cloud effects likely are more important for ocean glint observations than for land nadir observations since nearest cloud distances are smaller over the ocean than land (see Fig. 13). We assert that the predominant presence of QF1 data over the Amazon, which is subject to many low altitude clouds, is in part due to the difficulties imposed by 3D radiative transfer upon the 1D interpretation of measured Amazon OCO-2 radiances.

Data availability. The data used to generate the Fig. 4 curves can be downloaded from the Zenodo archive https://doi.org/10.5281/zenodo.7388228, and the 3D metric files are available at the archive https://doi.org/10.5281/zenodo.4008765

Author Contribution. Steven Massie performed the calculations presented in this paper, and was the primary author of the text. Heather Cronk supplied the MODIS-based nearest cloud distance data. Aronne Merrelli generated the 3D metric files. Steffen Mauceri and Sebastian Schmidt provided suggestions on the content of the paper.

Competing interests. At least one of the (co-)authors is a member of the editorial board of Atmospheric Measurement Techniques.

Acknowledgements. STM and KSS acknowledges support by NASA Grant 80NSSC21K1063 "Mitigation of 3D cloud radiative effects in OCO-2 and OCO-3 XCO2 retrievals". AM acknowledges support by JPL subcontract 1678415 and NASA Grant 80NSSC22K1287. Appreciation is expressed to the OCO-2 computer staff at the Jet Propulsion Laboratory, and to Garth D'Attillo and Timothy Fredrick of the Atmospheric Chemistry Observations and Modeling (ACOM) division at the National Center for Atmospheric Research (NCAR), supported by the National Science Foundation, for maintaining the operational capabilities of computer systems during the ongoing global COVID-19 pandemic.

https://doi.org/10.5194/amt-2022-323
Preprint. Discussion started: 14 December 2022

Atmospheric Measurement Techniques Discussions

References

Cronk, H.: OCO-2/MODIS Collocation Products User Guide, Version 3, June 2018, available at: ftp://ftp.cira.colostate.edu/ftp/ TTaylor/publications/ (last access: 19 February 2021), 2018.

Crisp, D., Pollock, H.R., Rosenberg, R., Chapsky, L., Lee, R.A., Oyafuso, F.A., Frankenberg, C., O'Dell, C.W., Bruegge, C.J., Doran, G.B. and Eldering, A.,:The on-orbit performance of the Orbiting Carbon Observatory-2 (OCO-2) instrument and its radiometrically calibrated products. *Atmospheric Measurement Techniques*, *10*(1), pp.59-81,2017.

Eldering, A., O'Dell, C. W., Wennberg, P. O., Crisp, D., Gunson, M. R., Viatte, C., Avis, C., Braverman, A., Castano, R., Chang, A., Chapsky, L., Cheng, C., Connor, B., Dang, L., Doran, G., Fisher, B., Frankenberg, C., Fu, D., Granat, R., Hobbs, J., Lee, R.A.M., Mandrake, L., McDuffie, J., Miller, C. E., Myers, V., Natraj, V., O'Brien, D., Osterman, G. B., Oyafuso, F., Payne, V. H., Pollock, H.R., Polonsky, I., Roehl, C.M., Rosenberg, R., Schwandner, F., Smyth, M., Tang, V., Taylor, T. E., To, C., Wunch, D., and Yoshimizu, J.: The Orbiting Carbon Observatory-2: first 18 months of science data products, Atmos. Meas. Tech., 10, 549– 563, https://doi.org/10.5194/amt-10-549-2017, 2017.

Emde, C.: Impact of 3D Cloud Structures on the Atmospheric Trace Gas Products from UV-VIS Sounders: Synthetic dataset for validation of trace gas retrieval algorithms, Zenodo [data set], https://doi.org/10.5281/zenodo.5567616, 2021.

Emde, C., Yu, H., Kylling, A., van Roozendael, M., Stebel, K., Veihelmann, B. and Mayer, B.: Impact of 3D cloud structures on the atmospheric trace gas products from UV–Vis sounders–Part 1: Synthetic dataset for validation of trace gas retrieval algorithms. *Atmospheric Measurement Techniques*, *15*(5), pp.1587-1608, 2022.

Evans, K.F.: The spherical harmonics discrete ordinate method for three-dimensional atmospheric radiative transfer, Atmos. Sci., 55, 429–446, 1998.

Massie, S. T., Schmidt, K. S., Eldering, A., and Crisp, D.: Observational evidence of 3-D cloud effects in OCO-2 CO2 retrievals, J. Geophys. Res. Atmos., 122, doi:10.1002/ 2016JD026111, 2017.

Massie,S. T., Cronk, H., Merrelli, A., O'Dell, C., Schmidt, K. Sebastian, Chen, H., and Baker D.: Analysis of 3D Cloud Effects in OCO-2 XCO2 Retrievals, Atmos. Meas. Tech., 14, 1475-1499, https://doi.org/10.5194/amt-14-1475-2021, 2021.

Merrelli, A., Bennartz, R., O'Dell, C.W., and Taylor, T. E.: Estimating bias in the OCO-2 retrieval algorithm caused by 3-D radiation scattering from unresolved boundary layer clouds, Atmos. Meas. Tech., 8, 1641–1656, https://doi.org/10.5194/amt-8-1641-2015, 2015.

Mishchenko, M. I., and Travis, L. D.: Satellite retrieval of aerosol properties over the ocean using polarization as well as intensity of reflected sunlight. J. Geophys. Res. Atmos., 102(D14), 16989-17013, 1997.

https://doi.org/10.5194/amt-2022-323
Preprint. Discussion started: 14 December 2022

OCO-2 L2 ATBD: Orbiting Carbon Observatoruy-2 & 3 (OCO-2 & OCO-3) Level 2 Full Physics Retrieval Algorithm Theoretical Basis, Version 2.0 Rev 3 January 2, 2019, JPL, California Institute of Technology, Pasadena, California, USA, 2019.

OCO-2 L2 ATBD: Orbiting Carbon Observatoruy-2 & 3 (OCO-2 & OCO-3) Level 2 Full Physics Retrieval Algorithm Theoretical Basis, Version 2.0 Rev 3 December 1, 2020, JPL, California Institute of Technology, Pasadena, California, USA, 2020.

O'Dell, C. W., Eldering, A., Wennberg, P. O., Crisp, D., Gunson, M. R., Fisher, B., Frankenberg, C., Kiel, M., Lindqvist, H., Mandrake, L., Merrelli, A., Natraj, V., Nelson, R. R., Osterman, G. B., Payne, V. H., Taylor, T. E., Wunch, D., Drouin, B. J., Oyafuso, F., Chang, A., McDuffie, J., Smyth, M., Baker, D. F., Basu, S., Chevallier, F., Crowell, S. M. R., Feng, L., Palmer, P. I., Dubey, M., García, O. E., Griffith, D. W. T., Hase, F., Iraci, L. T., Kivi, R., Morino, I., Notholt, J., Ohyama, H., Petri, C., Roehl, C. M., Sha, M. K., Strong, K., Sussmann, R., Te, Y., Uchino, O., and Velazco, V. A.: Improved retrievals of carbon dioxide from Orbiting Carbon Observatory-2 with the version 8 ACOS algorithm, Atmos. Meas. Tech., 11, 6539–6576, https://doi.org/10.5194/amt-11-6539-2018, 2018.

Payne, V. H., Drouin, B. J., Oyafuso, F., Kuai, L., Fisher, B. M., Sung, K., Nemchick, D., Crawford, T. J., Smyth, M., Crisp, D., Adkins, E.: Absorption coefficient (ABSCO) tables for the Orbiting Carbon Observatories: version 5.1. Journal of Quantitative Spectroscopy and Radiative Transfer, Nov 1;255:107217, 2020.

Pincus, R., and Evans, K. F.: Computational cost and accuracy in calculating three-dimensional radiative transfer: Results for new implementations of Monte Carlo and SHDOM, J. Atmos. Sci., 66, 3131–3146, 2009.

Rodgers, C. D.: Inverse Methods for Atmospheric Sounding: Theory and Practice, World Scientific, Singapore, 2000.

Taylor, T. E., O'Dell, C. W., Frankenberg, C., Partain, P. T., Cronk, H. Q., Savtchenko, A., Nelson, R. R., Rosenthal, E. J., Chang, A. Y., Fisher, B., Osterman, G. B., Pollock, R. H., Crisp, D., Eldering, A., and Gunson, M. R.: Orbiting Carbon Observatory-2 (OCO-2) cloud screening algorithms: validation against collocated MODIS and CALIOP data, Atmos. Meas. Tech., 9, 973–989, https://doi.org/10.5194/amt-9-973-2016, 2016.

Várnai, T., and A. Marshak, A.: MODIS observations of enhanced clear sky reflectance near clouds, Geophys. Res. Lett., 36, L06807, doi:10.1029/2008GL037089,2009.

Wunch, D., Wennberg, P. O., Osterman, G., Fisher, B., Naylor, B., Roehl, C. M., O'Dell, C., Mandrake, L., Viatte, C., Kiel, M., Griffith, D. W. T., Deutscher, N. M., Velazco, V. A., Notholt, J., Warneke, T., Petri, C., De Maziere, M., Sha, M. K., Sussmann, R., Rettinger, M., Pollard, D., Robinson, J., Morino, I., Uchino, O., Hase, F., Blumenstock, T., Feist, D. G., Arnold, S. G., Strong, K., Mendonca, J., Kivi, R., Heikkinen, P., Iraci, L., Podolske, J., Hillyard, P. W., Kawakami, S., Dubey, M. K., Parker, H. A., Sepulveda, E., García, O. E., Te, Y., Jeseck, P., Gunson, M. R., Crisp,

https://doi.org/10.5194/amt-2022-323
Preprint. Discussion started: 14 December 2022

Atmospheric Measurement Techniques Discussions

D., and Eldering, A.: Comparisons of the Orbiting Carbon Observatory-2 (OCO-2) XCO2 measurements with TCCON, Atmos. Meas. Tech., 10, 2209–2238, https://doi.org/10.5194/amt-10-2209-2017, 2017.

780

https://doi.org/10.5194/amt-2022-323
Preprint. Discussion started: 14 December 2022

Atmospheric Measurement Techniques Discussions

Table 1. Baseline and perturbations of the Fig. 5 calculations.

Case	Baseline	Perturbation
Surface pressure (hPa)	988.719	2 hPa
O2 surface reflectance	0.2536	0.025
WCO2 surface reflectance	0.140	0.014
SCO2 surface reflectance	0.043	0.0043
O2 aerosol optical depth	0.064	0.0064
WCO2 aerosol optical depth	0.037	0.0037
SCO2 aerosol optical depth	0.027	0.0027
XCO2	402.29	1 ppm

785

https://doi.org/10.5194/amt-2022-323
Preprint. Discussion started: 14 December 2022

Atmospheric Measurement Techniques Discussions

Table 2. Statistics of various fractional quantities for single day and 2016 yearly averages based upon an analysis of L2ABP preprocessor data files.

	Amazon Nadir 150622	Pacific Glint 160612	Amazon Nadir 2016	Amazon Glint 2016	Pacific Glint 2016
Latitude range	10 S – 3 N	8 N – 22 N	10 S – 3N	10 S – 3N	10 N – 20N
Longitude range	64 – 45 W	156 – 176 E	65 – 45 W	65 – 45 W	160 – 170E
Total Number Obs[a]	5162	6004	602939	636240	547808
Number of Retrievals[b]	589	4320	58477	77366	276944
Fraction Retrieved	0.11	0.71	0.096	0.12	0.50
Fraction QF0	0.40	0.55	0.43	0.34	0.60
Fraction QF1	0.60	0.44	0.56	0.65	0.39
Fraction Cloud< 4km[c]	0.80	0.50	0.56	0.53	0.56
Fraction Geom, 2km[d]	0.0	0.0	0.0	0.001	0.012
Fraction Geom, 4 km	0.0	0.0	0.005	0.009	0.021
Fraction Geom, 6 km	0.011	0.011	0.010	0.026	0.029
Fraction Geom, 8 km	0.013	0.014	0.012	0.037	0.034

a Total Number Obs is the total number of observations in the latitude – longitude range as specified by the L2ABP file.

b Number of retrievals is the number of successful retrievals as specified by the Lite file.

c Fraction Cloud < 4km is the fraction of retrievals for which the cloud distance is less than 4km.

d Fraction Geom, 2km is the fraction of retrievals associated with cloud shadows for the cloud height in 0 to 2km altitude range.

https://doi.org/10.5194/amt-2022-323
Preprint. Discussion started: 14 December 2022

Atmospheric Measurement Techniques Discussions

800

Table 3. Specifics of the multiple scenes.

Scene	Latitude	Longitude	Solar zenith angle	Sensor zenith angle
OG[a] 160612[b]	15.50	166.65	20	16
OG 160612	10.56	167.78	24	19
OG 160612	10.22	-128.78	24	19
OG 160612	5.26	-127.69	28	22
OG 160612	-10.13	-124.53	41	32
OG 160612	-14.28	-123.64	44	35
OG 160612	-17.55	-161.62	47	37
OG 160612	-26.15	-121.23	55	43
OG 160611	7.87	-142.19	26	20
OG 160611	5.77	-141.80	27	22
OG 160611	10.71	-142.85	24	19
OG 160611	11.48	-143.00	23	18
LN 150622	3.82	-58.18	30	0
LN 150622	0.45	-57.44	32	0
LN 150622	-5.24	-56.23	37	0
LN 150622	-5.87	-56.07	38	0
LN 150622	-6.52	-55.98	38	0
LN 150622	-8.58	-55.15	40	0
LN 160308	-11.78	-48.57	24	0
LN 160308	-18.11	-47.15	27	0
LN 160308	-21.08	-46.47	29	0
LN 160107	-23.29	-53.65	24	0
LN 160107	-16.96	-55.16	24	0
LN 160107	-25.44	-53.18	24	0
LG 150625	-2.31	-65.89	34	27
LG 150625	-4.03	-65.51	35	28
LG 150625	-1.20	-66.13	33	26
LG 150625	3.53	-67.08	29	23
LG 200603	-3.57	-57.89	35	27
LG 200603	1.99	-59.09	30	24
LG 200603	0.35	-58.77	31	24
LG 200603	2.89	-59.24	29	23

https://doi.org/10.5194/amt-2022-323
Preprint. Discussion started: 14 December 2022

Atmospheric Measurement Techniques Discussions

LG 200610	-10.59	-58.04	41	32
LG 200610	-9.44	-58.21	40	31
LG 200610	-3.69	-59.39	35	28
LG 200610	-1.45	-59.87	33	26

805

a OG, LN, and LG refer to ocean glint, land nadir, and land glint observing modes

b 160612 refers to June 12, 2016

https://doi.org/10.5194/amt-2022-323
Preprint. Discussion started: 14 December 2022

Atmospheric Measurement Techniques Discussions

Table 4. Ranges (minimum, average, maximum) of the six curves in Figure 17.

Curve	Minimum	Average	Maximum
For 50°° S to 50 N			
Ocean glint QF0	-0.11[a]	0.42	0.62
Land glint QF0	-1.34	-0.02	0.44
Land nadir QF0	-1.01	-0.05	0.58
Ocean glint QF1	1.04	1.59	2.33
Land glint QF1	0.42	1.66	2.67
Land nadir QF1	-0.05	1.28	2.66
For 50° S to 0° N			
Ocean glint QF0	0.43	0.52	0.56
Land glint QF0	0.02	0.25	0.44
Land nadir QF0	-0.21	0.23	0.57
Ocean glint QF1	1.04	1.42	2.33
Land glint QF1	1.80	2.18	2.67
Land nadir QF1	1.34	1.98	2.66
For 0° N to 50° N			
Ocean glint QF0	-0.11	0.34	0.62
Land glint QF0	-1.34	-0.25	0.44
Land nadir QF0	-1.01	-0.29	0.49
Ocean glint QF1	1.56	1.72	1.96
Land glint QF1	0.42	1.22	2.64
Land nadir QF1	-0.05	0.70	2.23

a values are in ppm

https://doi.org/10.5194/amt-2022-323
Preprint. Discussion started: 14 December 2022

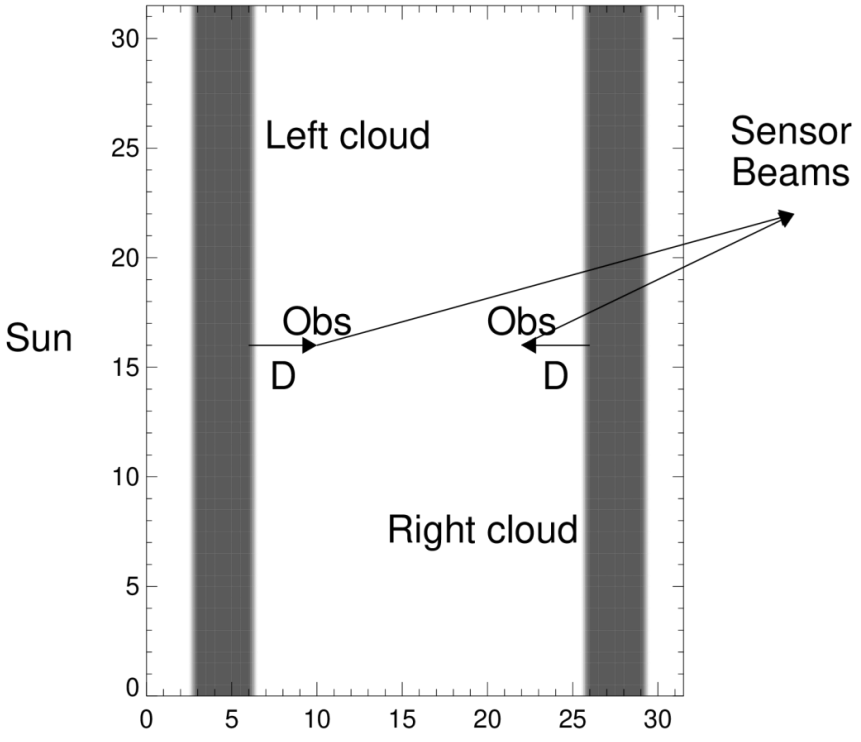

Figure 1. Idealized bar clouds for a cloud height of 1.4 km. The Sun and OCO2 are to the left and right of the 32 km x 32 km SHDOM scene, and two observation points are distance D from the Left and Right clouds. Two sensor beams are indicated by the upward sloping arrows.

https://doi.org/10.5194/amt-2022-323
Preprint. Discussion started: 14 December 2022

Atmospheric Measurement Techniques Discussions

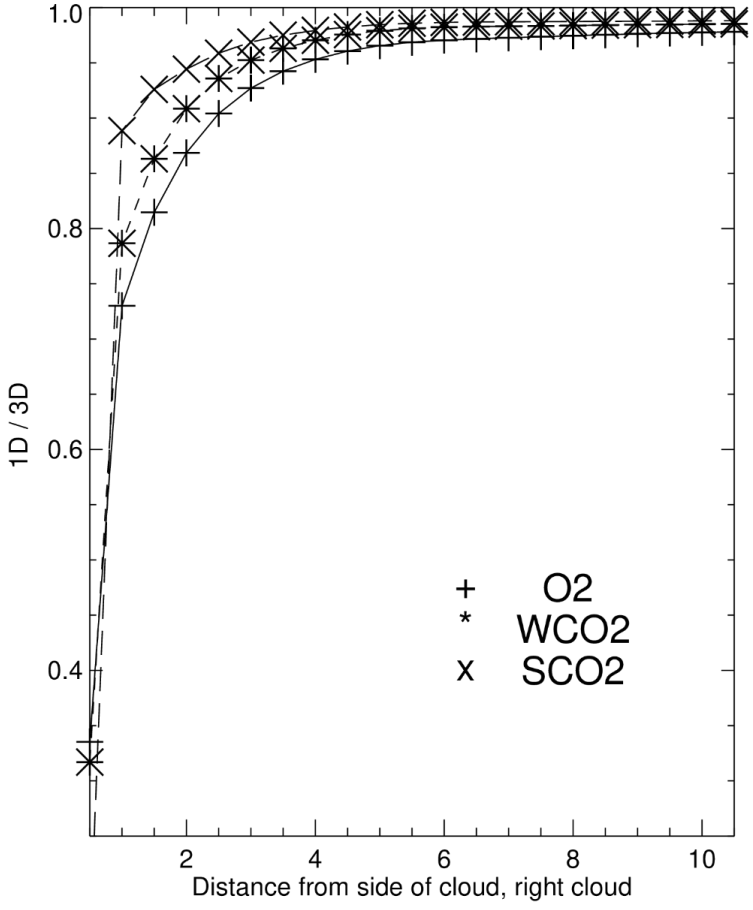

825 **Figure 2**. Illustration of 1D / 3D intensity ratios as a function of distance D from the Right cloud in Fig. 1. 3D cloud effects are present in all three OCO-2 bands, with largest effects (smallest 1D / 3D ratios) in the O2 A-band. The ABSCO vertical gas optical depth is near 0.01, and the azimuth angle is 180°.

https://doi.org/10.5194/amt-2022-323
Preprint. Discussion started: 14 December 2022

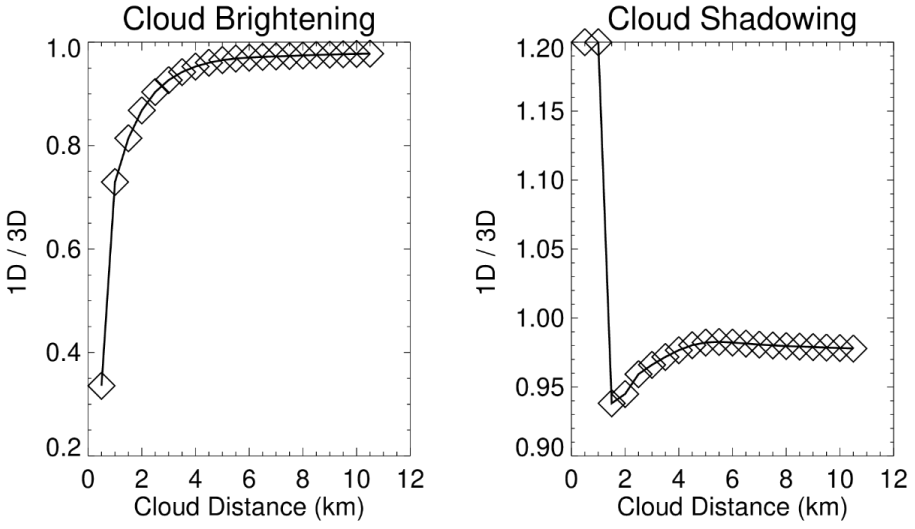

Figure 3 1D / 3D intensity ratios as a function of distance D from Right (left panel) and Left (right panel) idealized bar clouds, for the O2 A-band continuum (vertical gas optical depth is 0.0008). Cloud shadows are present in the right panel, and 3D cloud brightening is present in the left panel. The idealized bar clouds have the same altitude, pressure, temperature profile as that of the detailed SHDOM calculation of Fig. 6 for June 22, 2015 at 6.52° S and longitude -55.98° W.

https://doi.org/10.5194/amt-2022-323
Preprint. Discussion started: 14 December 2022

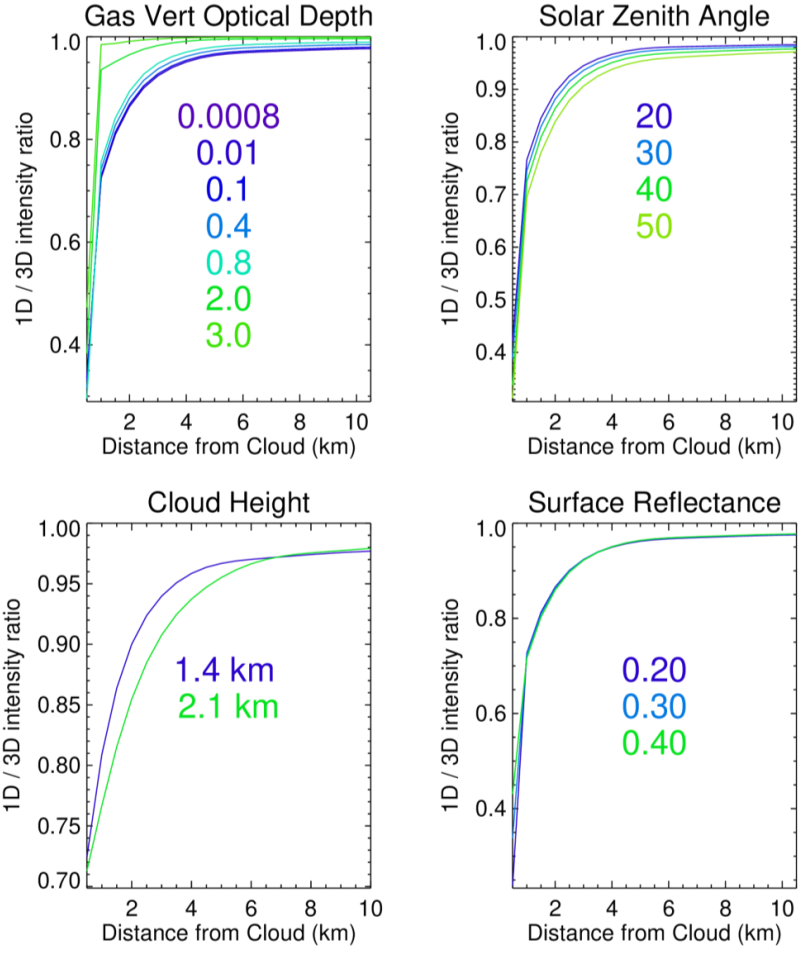

Figure 4. Upper left: Dependence of O2 A-band 1D / 3D ratios on the ABSCO gas vertical optical depth and as a function of nearest cloud distance. There is a sharp kink for the x=0.5 and x=1.0 km data points for optical depths near 1 and 2 since the x grid is in 0.5 km increments. The cloud top height is 1.4 km, the Lambertian surface reflectance is 0.30, and the aerosol vertical optical depth is 0.16. Upper right: Dependence of 1D / 3D ratios on the solar zenith angle. The ABSCO gas vertical optical depth is 0.0008 and the Lambertian surface reflectance is 0.30. Lower left: Dependence of 1D / 3D ratios on cloud vertical thickness, labeled by the cloud top height, with a cloud base at 0.1 km. The ABSCO gas vertical optical depth is 0.0008, the Lambertian surface reflectance is 0.30, and the solar zenith angle is 40°. Lower right: Dependence of 1D /3D ratios on the Lambertian surface reflectance. The ABSCO gas vertical optical depth is 0.0008 and the solar zenith angle is 40°.

https://doi.org/10.5194/amt-2022-323
Preprint. Discussion started: 14 December 2022

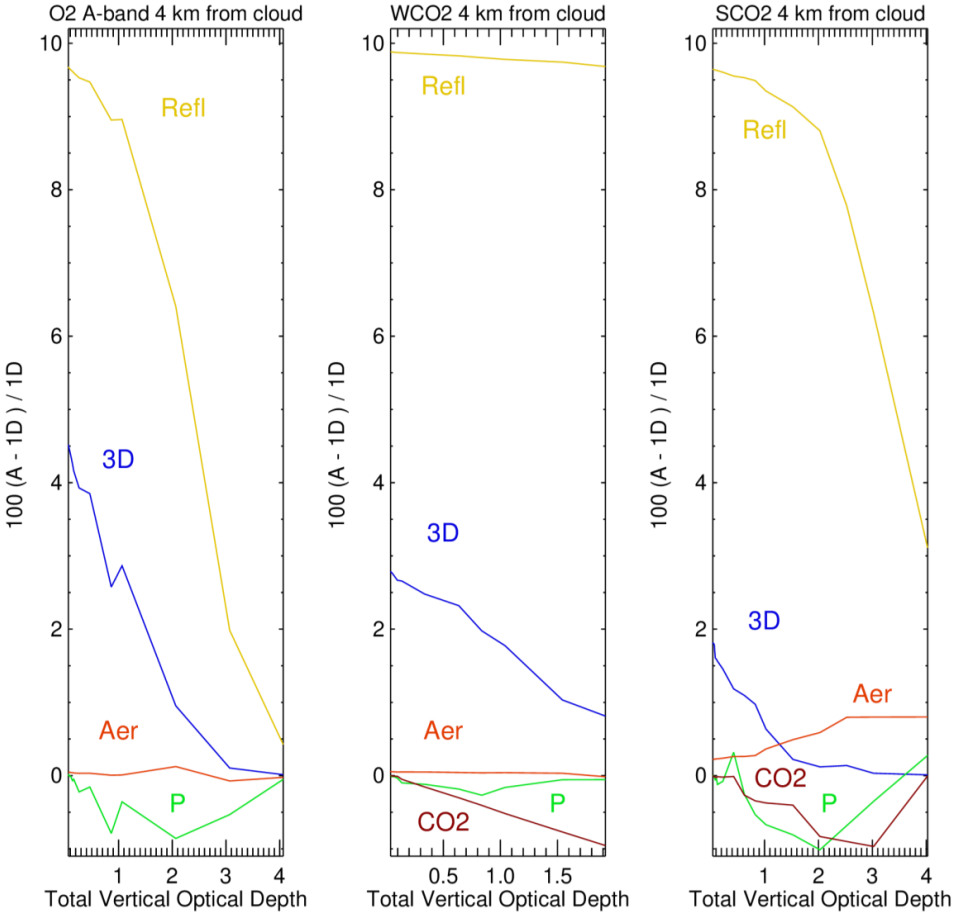

855 **Figure 5**. Radiance perturbations based upon an Amazon nadir scene atmospheric profile using idealized bar clouds. The observation point is 4 km from the cloud. "A" in the y axis label stands for the 1D perturbation radiance or the 3D radiance. Aerosol (Aer) optical depths and surface reflectivity (Refl) are perturbed by 10% from the Table 1 baseline values, while the surface pressure (P) is perturbed by 2 hPa and CO_2 in the WCO2 and SCO2 bands is perturbed by 1 ppm.

860

https://doi.org/10.5194/amt-2022-323
Preprint. Discussion started: 14 December 2022

Atmospheric Measurement Techniques Discussions

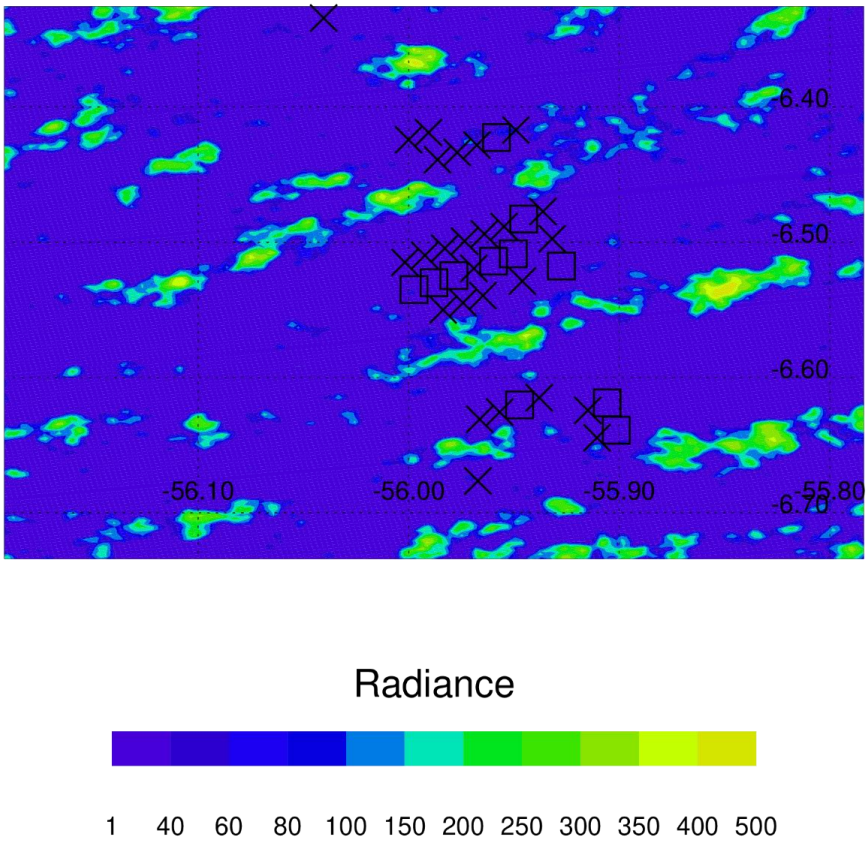

Figure 6. MODIS radiance field (units are W/m^2/sr/μm) on June 22, 2015 over the Amazon as a function of longitude and latitude, and the location of V10 Lite file observations, marked by the square □ (QF0), and X (QF1) symbols. The observations are between the clouds (the irregular green, yellow areas). The direction of the incident sunbeam is from the northwest.

https://doi.org/10.5194/amt-2022-323
Preprint. Discussion started: 14 December 2022

Atmospheric Measurement Techniques Discussions

870

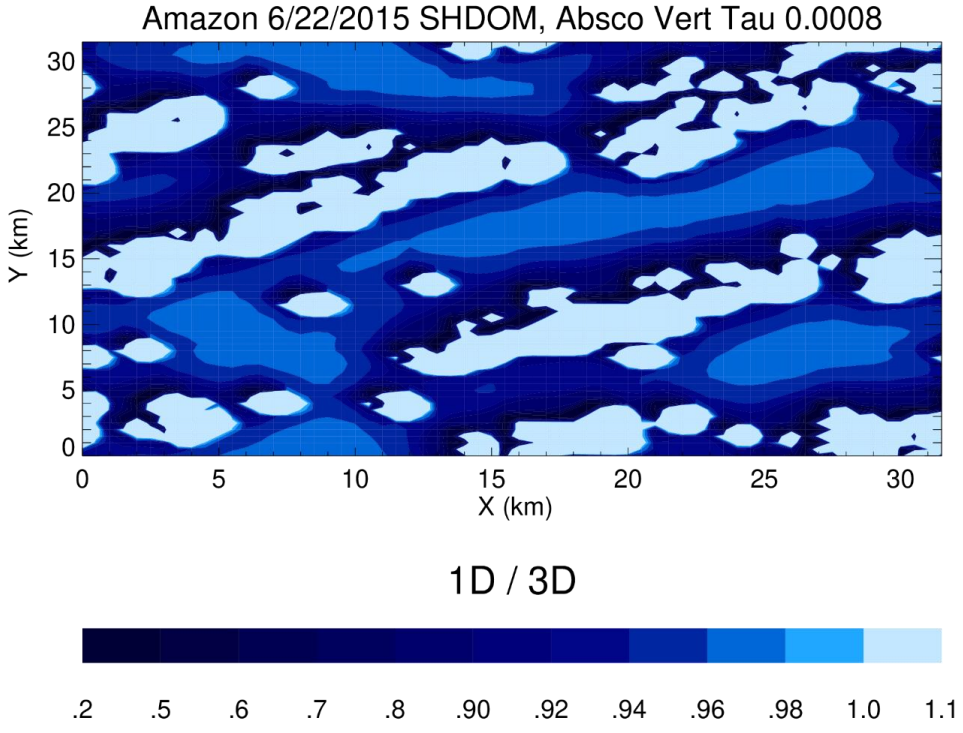

Figure 7. SHDOM calculation of 1D / 3D ratios for the June 22, 2015 Amazon scene. The smallest 1D / 3D ratios are located on the sunward side of clouds (white), with the direction of the incident sunbeam from the northwest.

875

https://doi.org/10.5194/amt-2022-323
Preprint. Discussion started: 14 December 2022

Atmospheric Measurement Techniques Discussions

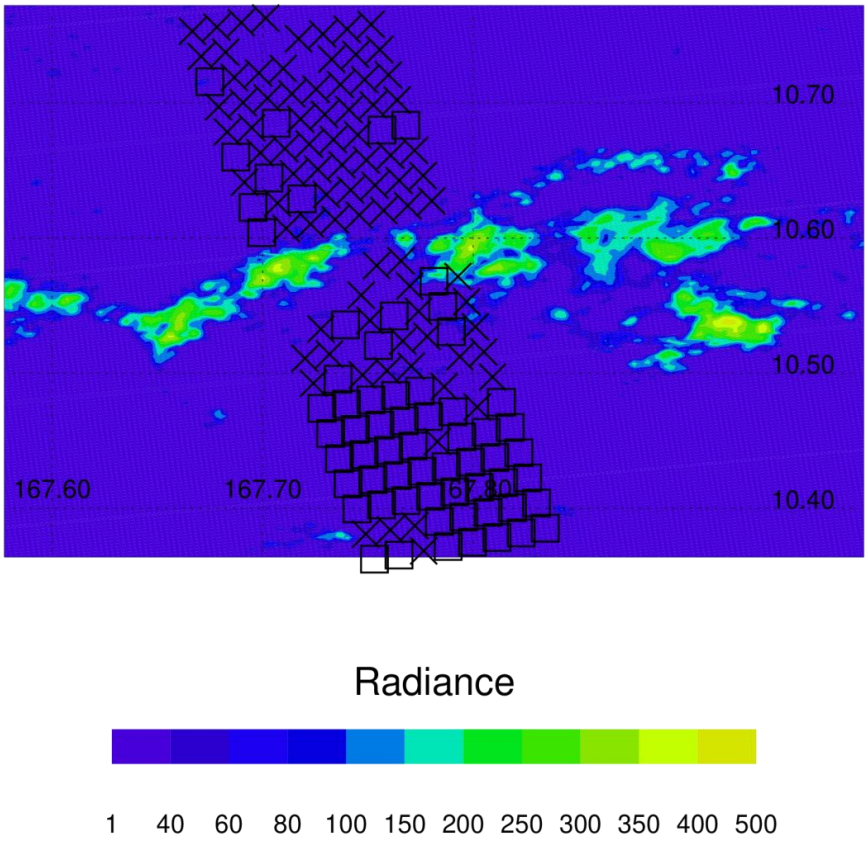

Figure 8. MODIS radiance field (units are W/m^2/sr/μm) on June 12, 2016 over the ocean as a function of longitude and latitude, and the location of V10 Lite file observations, marked by the square □ (QF0) and X (QF1) symbols. The observations are between the clouds (the irregular green, yellow areas). The direction of the incident sunbeam is from the northwest.

https://doi.org/10.5194/amt-2022-323
Preprint. Discussion started: 14 December 2022

Atmospheric Measurement Techniques Discussions

885

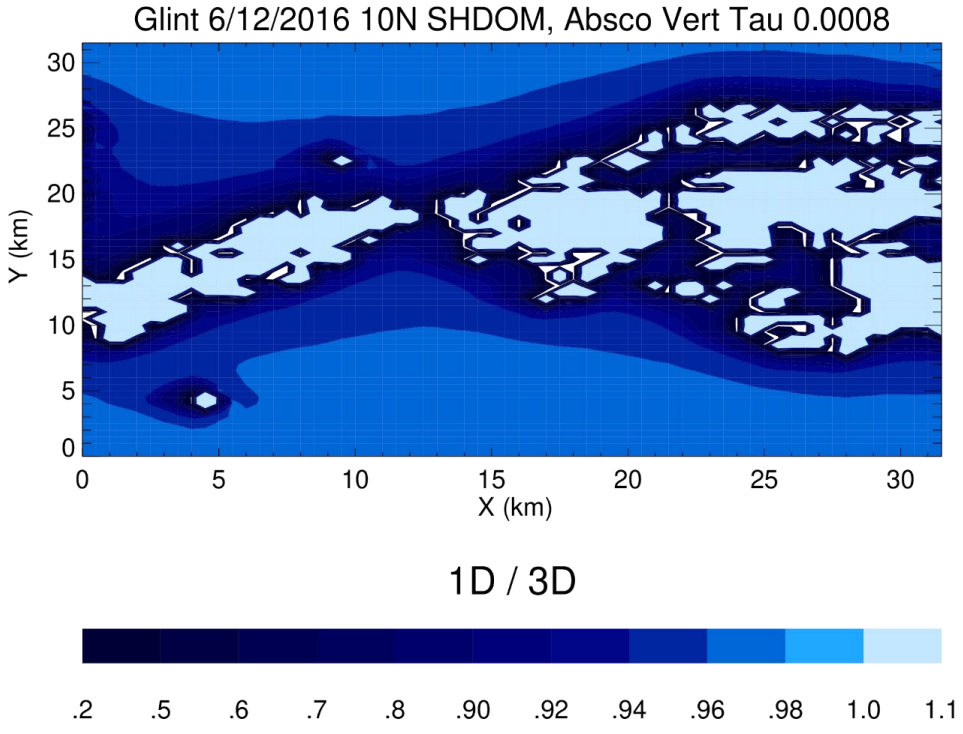

Figure 9. SHDOM 1D / 3D ratio field for the Fig. 8 ocean glint scene. Notice the increase in the 1D / 3D ratios as distance from clouds increases, with clouds corresponding to areas with 1D / 3D
890 ratios greater than unity.

https://doi.org/10.5194/amt-2022-323
Preprint. Discussion started: 14 December 2022

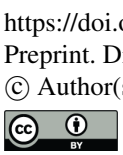

Atmospheric Measurement Techniques Discussions

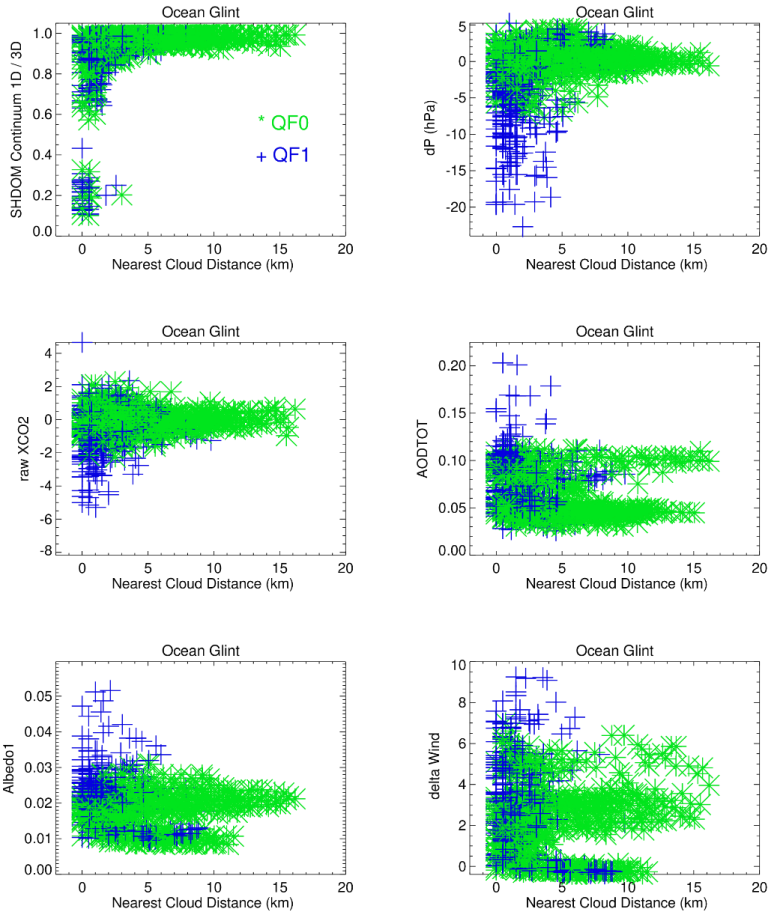

895 **Figure 10**. Individual Lite file QF=0 (*, green) and QF=1 (+, blue) SHDOM continuum 1D / 3d, OCO-2 dP, raw XCO2, total aerosol optical depth, Albedo1 (for the O2 A-band), and "delta Wind" (see text), as a function of nearest cloud distance for the 12 ocean glint scenes.

https://doi.org/10.5194/amt-2022-323
Preprint. Discussion started: 14 December 2022

Atmospheric Measurement Techniques Discussions

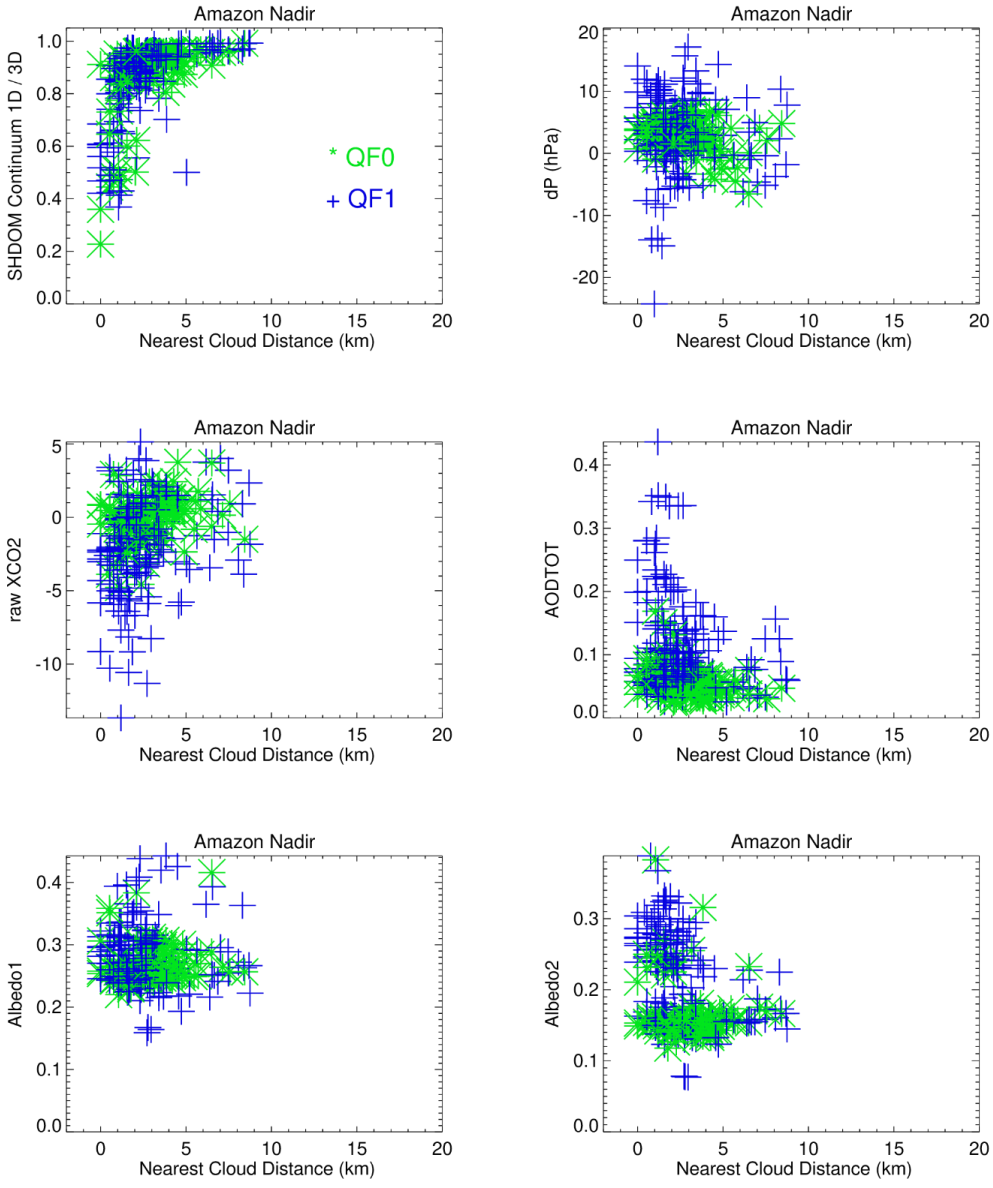

900

Figure 11. Individual Lite file QF=0 (*, green) and QF=1 (+, blue) SHDOM continuum 1D / 3D, OCO-2 dP, raw XCO2, total aerosol optical depth, Albedo1 (for the O2 A-band) and Albedo2 (for the WCO2 band) data as a function of nearest cloud distance for the 12 Amazon nadir scenes.

https://doi.org/10.5194/amt-2022-323
Preprint. Discussion started: 14 December 2022

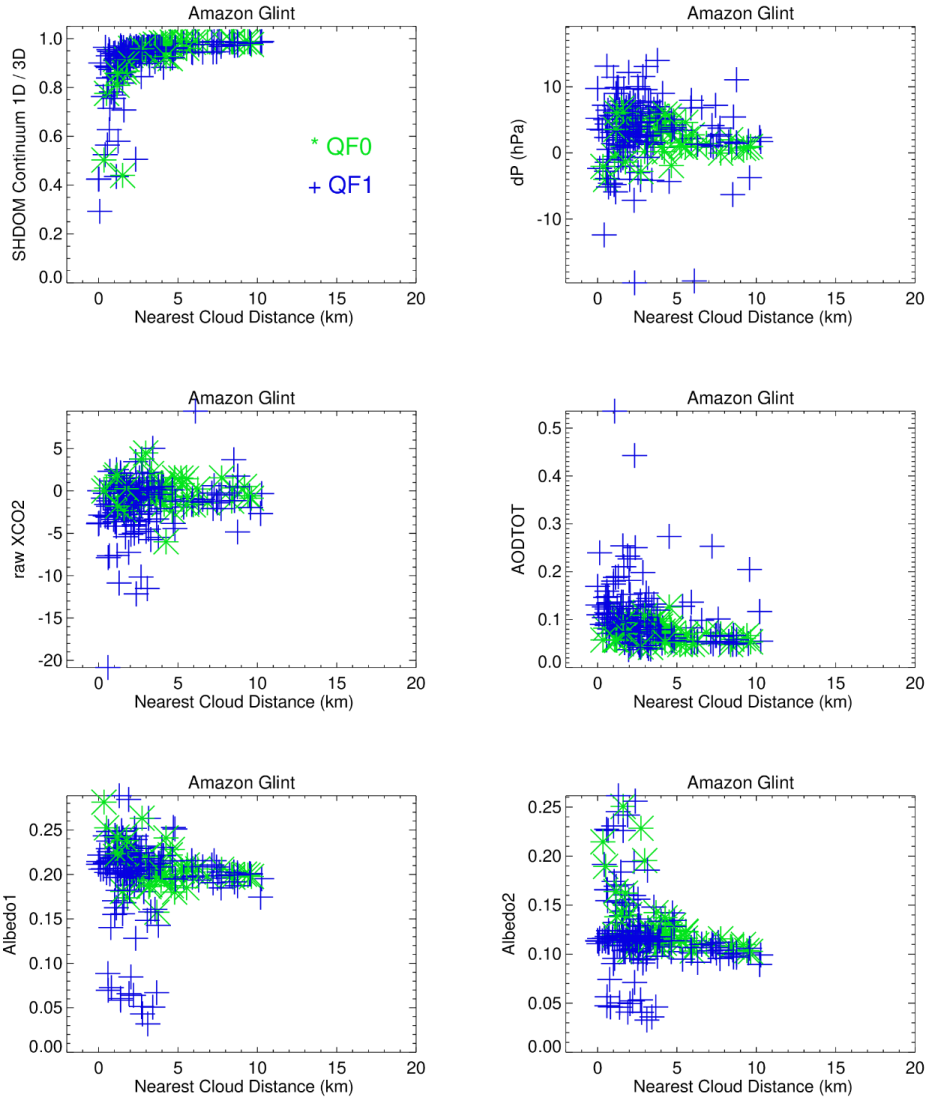

905 **Figure 12**. Individual Lite file QF=0 (*, green) and QF=1 (+, blue) SHDOM continuum 1D / 3D, OCO-2 dP, raw XCO2, total aerosol optical depth, Albedo1 (for the O2 A-band) and Albedo2 (for the WCO2 band) data as a function of nearest cloud distance for the 12 Amazon glint scenes.

910

https://doi.org/10.5194/amt-2022-323
Preprint. Discussion started: 14 December 2022

Atmospheric Measurement Techniques Discussions

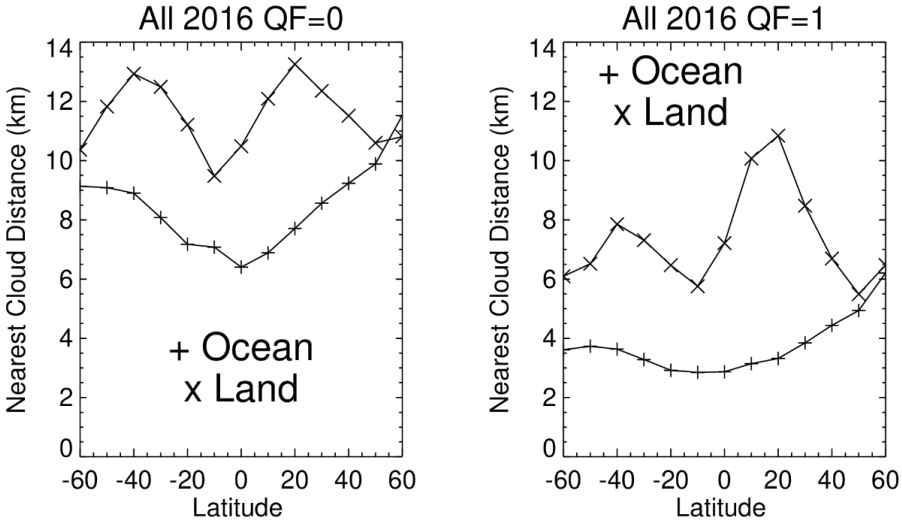

Figure 13. Zonal averages of nearest cloud distance over ocean and land for 2016 QF0 and QF1 data.

915

https://doi.org/10.5194/amt-2022-323
Preprint. Discussion started: 14 December 2022

Atmospheric Measurement Techniques Discussions

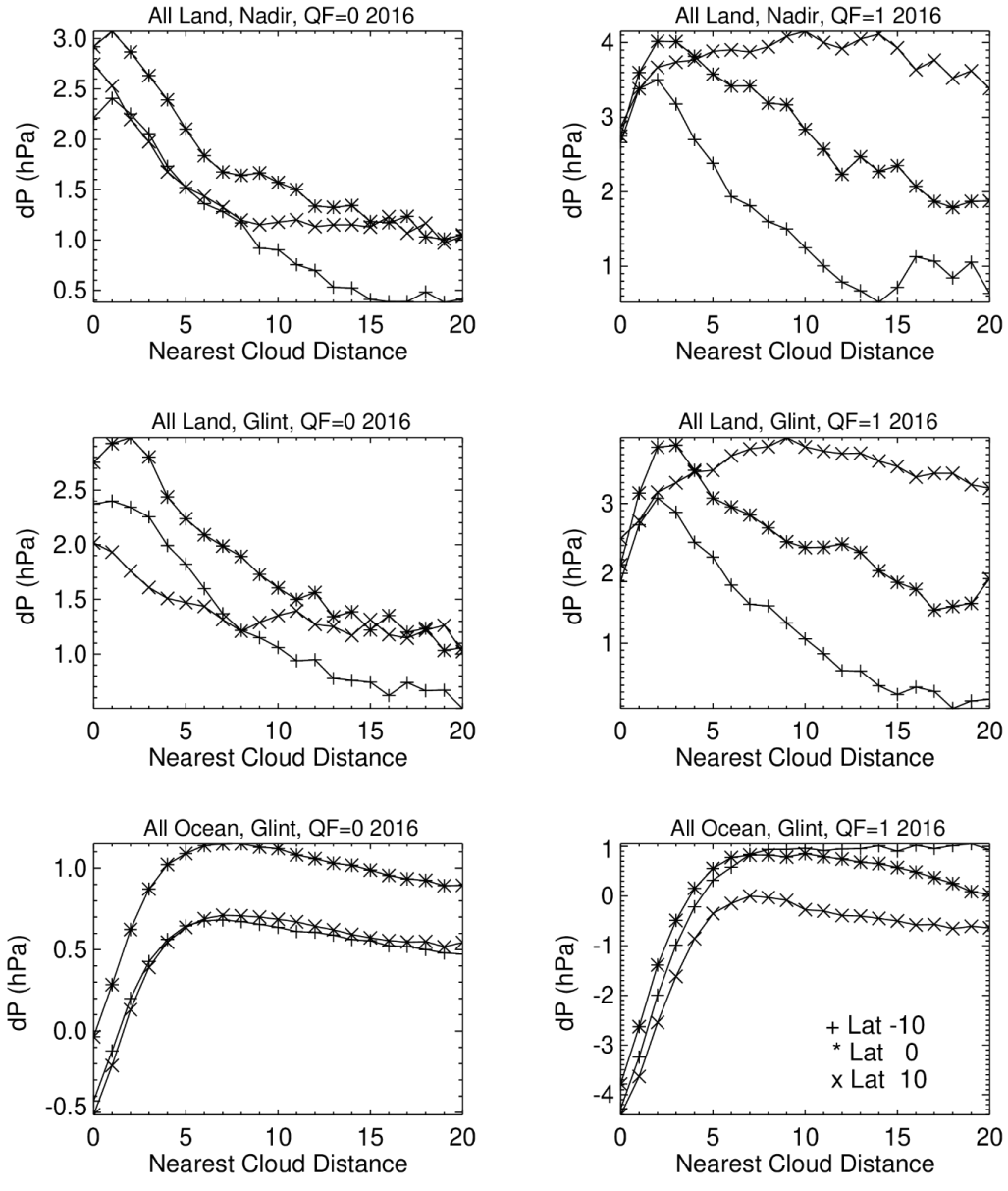

Figure 14. dP averages as a function of nearest cloud distance

920

https://doi.org/10.5194/amt-2022-323
Preprint. Discussion started: 14 December 2022

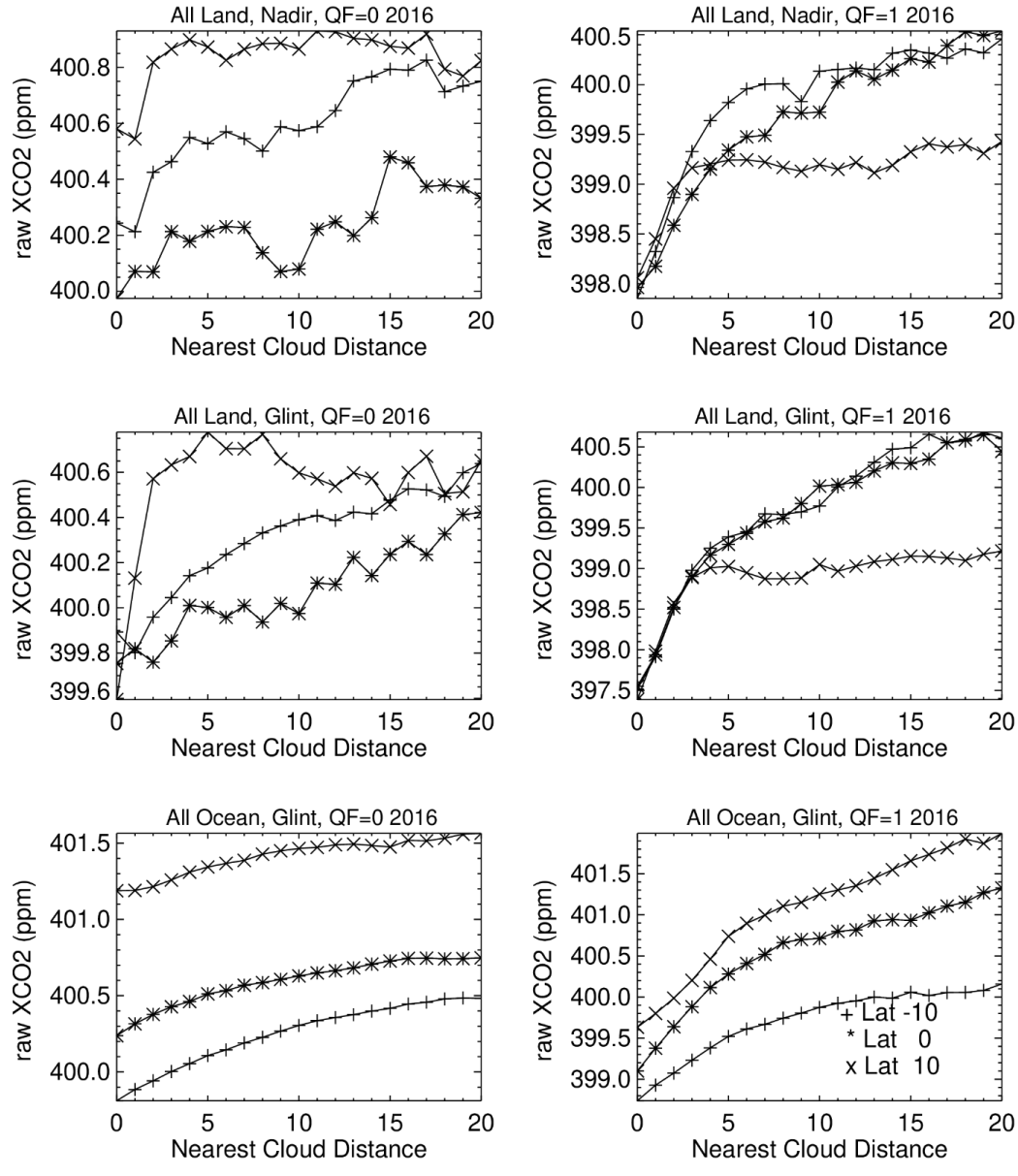

Figure 15. Raw XCO2 averages as a function of nearest cloud distance.

https://doi.org/10.5194/amt-2022-323
Preprint. Discussion started: 14 December 2022

Atmospheric Measurement Techniques Discussions

925

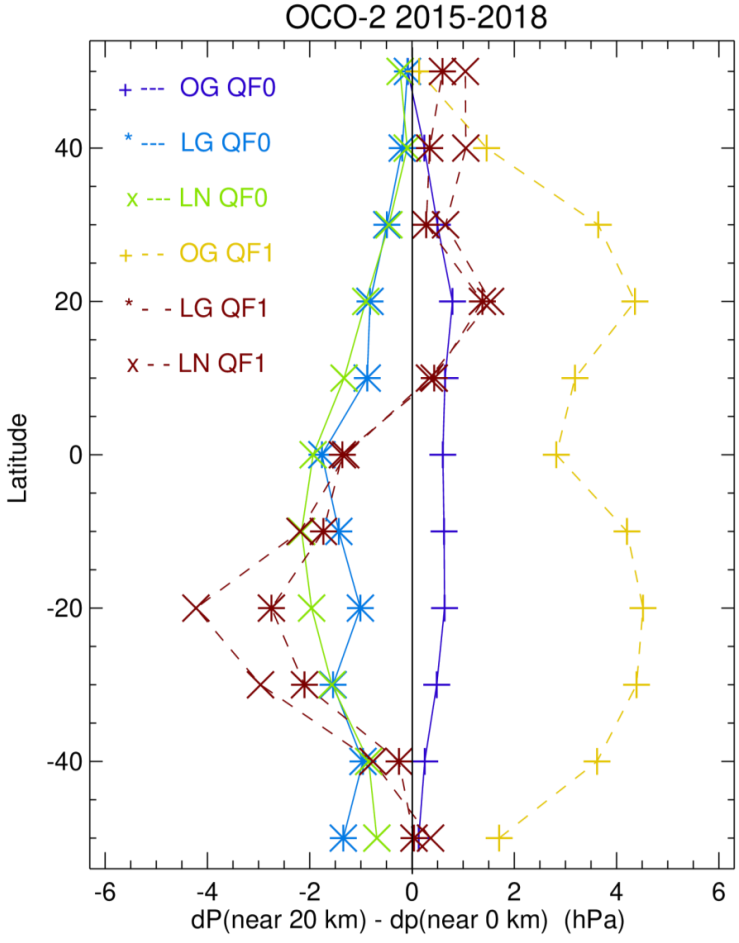

Figure 16. Latitudinal averages of dP (near 20 km) – dP (near 0 km) for 2015 – 2018 for QF0 (solid line) and QF1 (broken line) data. OG, LN, and LG refer to ocean glint, land nadir, and land glint observing modes.

930

https://doi.org/10.5194/amt-2022-323
Preprint. Discussion started: 14 December 2022

Atmospheric Measurement Techniques Discussions

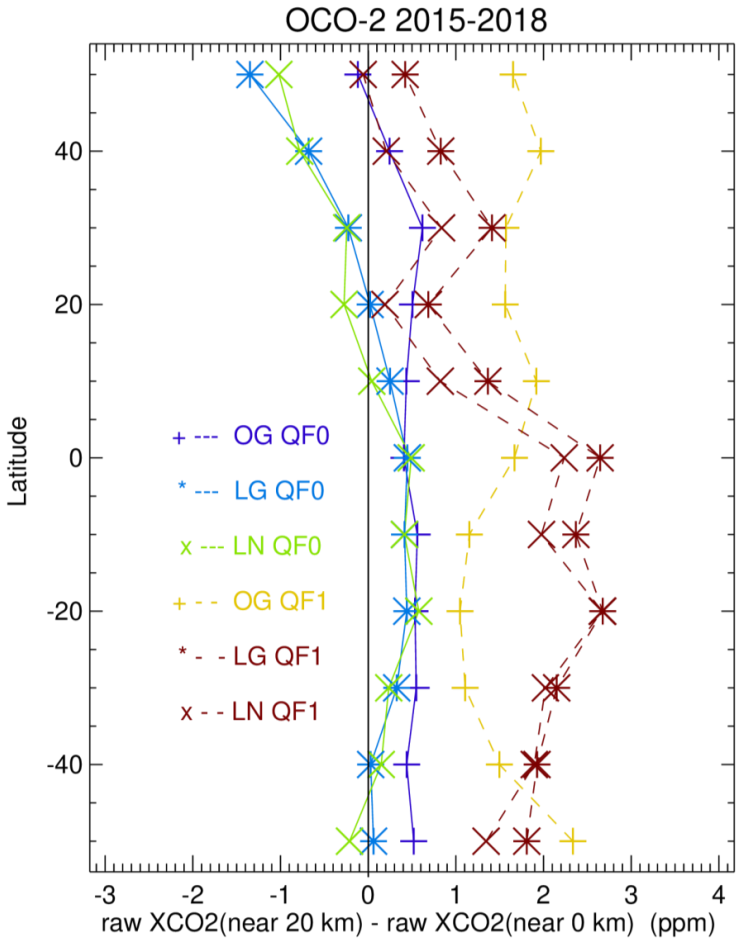

Figure 17. Latitudinal averages of raw XCO2 (near 20 km) – raw XCO2 (near 0 km) for 2015 – 2018 for QF0 (solid line) and QF1 (broken line) data. OG, LN, and LG refer to ocean glint, land nadir, and land glint observing modes.

935